## TLR activation
## Low Fatty Acid

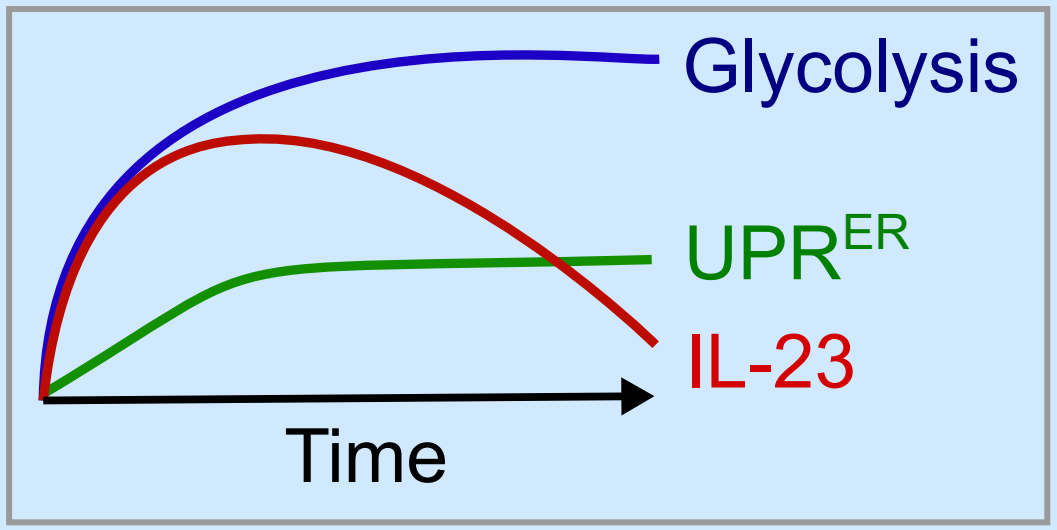


## TLR activation
## High Fatty Acid

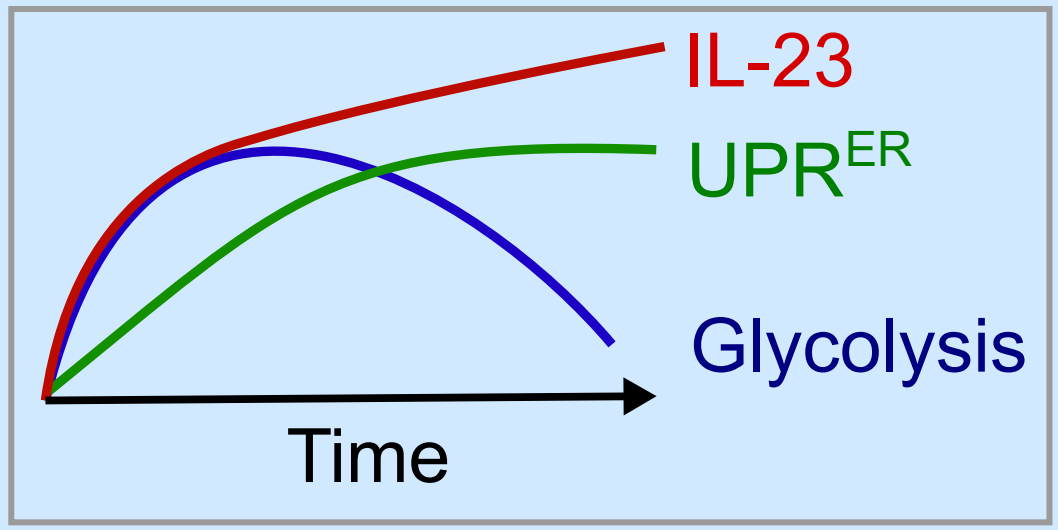


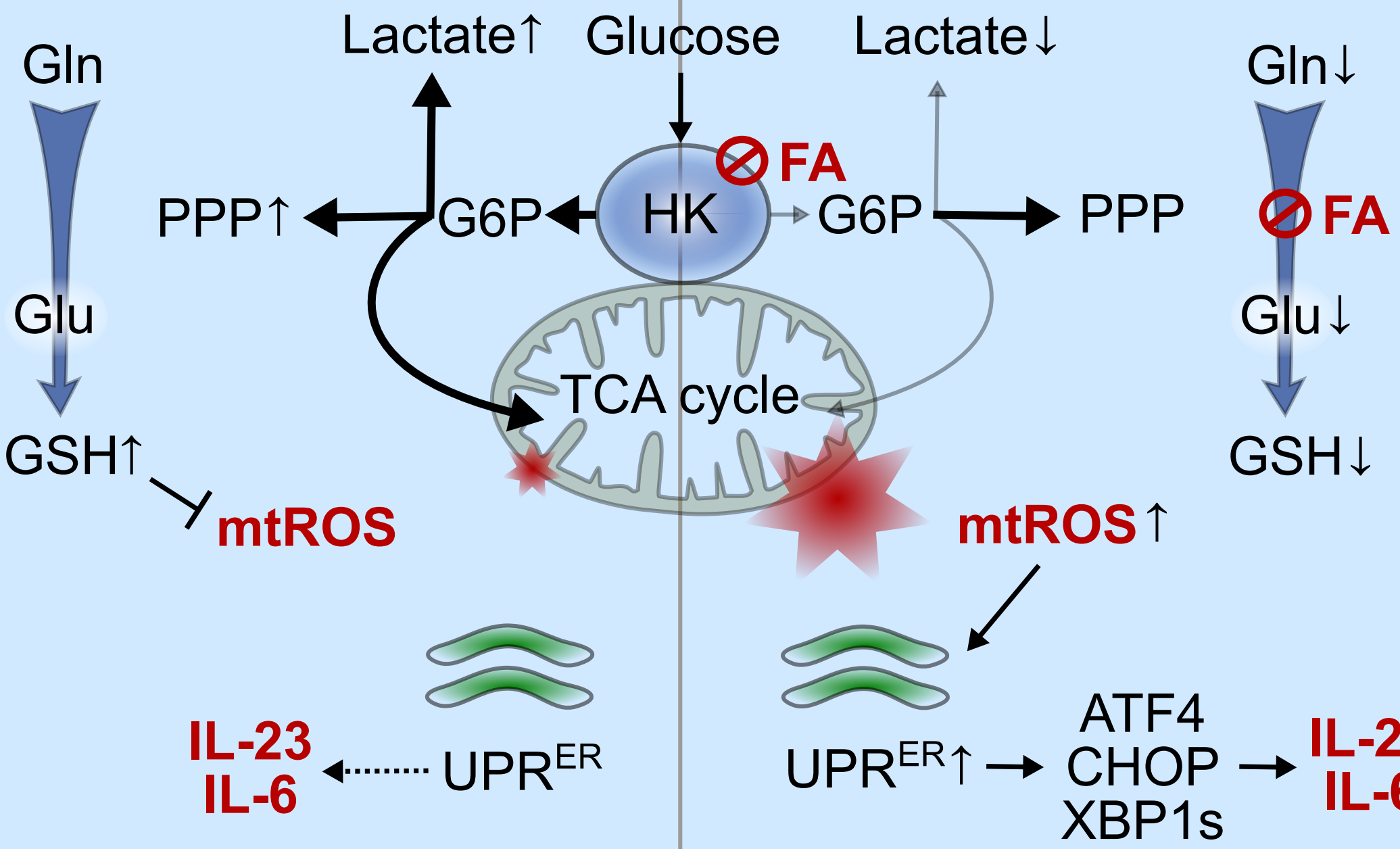


**Resolution of inflammation**

**Unresolved inflammation**

**Metabolic and innate immune cues merge into a specific inflammatory response via UPR**

Denis A. Mogilenko[1], Joel T. Haas[1], Laurent L'homme[1], Sébastien Fleury[1], Sandrine Quemener[1], Matthieu Levavasseur[1,2], Coralie Becquart[1,2], Julien Wartelle[1], Alexandra Bogomolova[1], Laurent Pineau[1], Olivier Molendi-Coste[1], Steve Lancel[1], Hélène Dehondt[1], Celine Gheeraert[1], Aurelie Melchior[1], Cédric Dewas[1], Artemii Nikitin[1], Samuel Pic[1], Nabil Rabhi[3], Jean-Sébastien Annicotte[3], Seiichi Oyadomari[4], Talia Velasco-Hernandez[5], Jörg Cammenga[5], Marc Foretz[6,7,8], Benoit Viollet[6,7,8], Milica Vukovic[9], Arnaud Villacreces[9], Kamil Kranc[9], Peter Carmeliet[10,11], Guillemette Marot[12], Alexis Boulter[13], Simon Tavernier[14], Luciana Berod[15], Maria P. Longhi[16], Christophe Paget[17], Sophie Janssens[18], Delphine Staumont-Sallé[1,2,21], Ezra Aksoy[19,21], Bart Staels[1, 21], David Dombrowicz[1,20*]

[1]University of Lille, EGID, Inserm, CHU Lille, Institut Pasteur de Lille, U1011, 59019 Lille, France.

[2]Department of Dermatology, CHU Lille, 59045 Lille, France.

[3]University of Lille, EGID, CNRS, CHU Lille, Institut Pasteur de Lille, UMR 8199, 59019 Lille, France

[4]Fujii Memorial Institute of Medical Sciences, Institute of Advanced Medical Sciences, Tokushima University, Tokushima, Japan 770-8503.

[5]Department of Hematology, Institute for Clinical and Experimental Medicine, Linköping University, 58185 Linköping, Sweden.

[6]Université Paris Descartes, Sorbonne Paris Cité, 75006 Paris, France.

[7]INSERM U1016, Institut Cochin, 75014 Paris France

[8]CNRS, UMR8104, 75014 Paris, France.

[9]Centre for Haemato-Oncology, Barts, and the London School of Medicine and Dentistry, Queen Mary University of London, London EC1M 6BQ, UK.

[10]Laboratory of Angiogenesis and Vascular Metabolism, Center for Cancer Biology, VIB, 3000 Leuven, Belgium.

[11]Laboratory of Angiogenesis and Vascular Metabolism, Department of Oncology, University of Leuven, Leuven, 3000 Belgium.

[12]Université Lille, MODAL Team, Inria Lille-Nord Europe, 59650 Villeneuve-d'Ascq, France.

[13]University of Florida College of Medicine, Gainesville, Florida 32610, USA

[14]Laboratory of Immunoregulation and Mucosal Immunology, VIB Center for Inflammation Research and Department of Internal Medicine and Pediatrics, Ghent University, 9052 Ghent, Belgium

[15]Institute of Infection Immunology, TWINCORE, Centre for Experimental and Clinical Infection Research, A Joint Venture between the Medical School Hannover (MHH) and the Helmholtz Centre for Infection Research (HZI), Hannover, Niedersachsen 30625, Germany.

[16]William Harvey Research Institute, Barts, and the London School of Medicine and Dentistry, Queen Mary University of London, London EC1M 6BQ, UK.
[17]Université de Tours, INSERM, Centre d'Etude des Pathologies Respiratoires (CEPR), UMR 1100, 37041 Tours, France.
[18]ER Stress and Inflammation, VIB Center for Inflammation Research, Ghent, Belgium and Department of Internal Medicine and Pediatrics, Ghent University, 9052 Ghent, Belgium
[19]Centre for Biochemical Pharmacology, William Harvey Research Institute, Queen Mary University of London, London EC1M 6BQ, UK.
[20]Lead Contact: David Dombrowicz. Inserm U1011. Institut Pasteur de Lille. 1, r. Prof. Camette BP245. 59019 Lille Cedex. France.
*Correspondence: david.dombrowicz@inserm.fr

**Summary**

Innate immune responses are intricately linked with intracellular metabolism of myeloid cells. Toll-like receptor (TLR) stimulation shifts intracellular metabolism toward glycolysis, while anti-inflammatory signals depend on enhanced mitochondrial respiration. How exogenous metabolic signals affect the immune response is unknown. We demonstrate that TLR-dependent responses of dendritic cells (DC) are exacerbated by a high fatty acid (FA) metabolic environment. FA suppress the TLR-induced hexokinase activity and perturb tricarboxylic acid cycle metabolism. These metabolic changes enhance mitochondrial reactive oxygen species (mtROS) production and, in turn, the unfolded protein response (UPR) leading to a distinct transcriptomic signature, with IL-23 as hallmark. Interestingly, chemical or genetic suppression of glycolysis was sufficient to induce this specific immune response. Conversely, reducing mtROS production or DC-specific deficiency in XBP1 attenuated IL-23 expression and skin inflammation in an IL-23-dependent model of psoriasis. Thus, fine-tuning of innate immunity depends on optimization of metabolic demands and minimization of mtROS-induced UPR.

**Introduction**

Metabolic adaptations play an important role in host response to pathogens (Wang et al., 2016; Weis et al., 2017). Inflammatory responses are triggered by pattern-recognition receptors (PRRs), such as Toll-like receptors (TLRs), which recognize pathogen-associated molecular patterns (PAMPs) (Medzhitov, 2001). Inflammation is a tightly controlled process sensitive to dynamic changes in tissue environment and to the intrinsic state of immune cells, both contributing to initiation and resolution of inflammation (Netea et al., 2017). However, dysregulation of the transient inflammatory response can result in chronic inflammatory diseases (Fullerton and Gilroy, 2016).

Recent evidence shows that metabolism of macrophages and DC plays a crucial role in inflammation (O'Neill and Pearce, 2016). Both DC and macrophages undergo a robust increase of glycolysis after acute activation by TLR agonists, whereas mitochondrial activity is suppressed in such conditions (Krawczyk et al., 2010; Tannahill et al., 2013). This shift of metabolic activity, known as glycolytic reprogramming, results in altered mitochondrial function, increased reactive oxygen species (ROS) production, and elevated secretion of pro-inflammatory cytokines (Tannahil et al., 2013; Lampropoulou et al., 2016; Mills et al., 2016). Importantly, processes that drive glycolytic reprogramming in M1 macrophages, activated by the TLR4 agonist LPS, are down-regulated in IL-4-polarized M2 macrophages (Jha et al., 2015) or in response to IL-10 (Ip et al., 2017). In addition, a recent study demonstrated that the key hallmarks of M2 macrophages are fatty acid oxidation (FAO)-independent and are not regulated by mitochondrial respiration (Divakaruni et al., 2018). Alterations of immune

signaling have a profound impact on whole body metabolism in metabolic diseases such as obesity and type 2 diabetes (Hotamisligil, 2017). Conversely, altered metabolic environment, for instance, due to obesity, affects myeloid cells during the innate inflammatory response (Duan et al., 2018). Immune cells sense environmental and metabolic cues that induce specialized stress responses in these cells (Chovatiya and Medzhitov, 2014). Flexibility of immune cells to adapt to different metabolic demands and diverse metabolic milieu via dynamic regulation of intracellular metabolism is an important component of inflammation and tissue homeostasis (Gaber et al., 2017). However, the underlying molecular mechanisms remain poorly understood. We hypothesized that metabolic adaptations during DC innate immune activation might be sensitive to extracellular metabolites such as FA, whose concentrations are altered by nutritional status and in several metabolic diseases (Karpe et al., 2011). Our results show that FA enhance TLR-mediated innate activation by inhibiting hexokinase (HK) thereby impairing the glycolytic reprogramming, leading to disturbed mitochondrial fitness and increased mtROS generation. This results in an exacerbated unfolded protein response (UPR) and, in turn, induces a distinct molecular signature and inflammatory response characterized by increased IL-23 production. Thus, adaptation of glycolysis to the metabolic environment links mtROS production to UPR activation and represents a specific mechanism regulating innate immunity.

## Results

### FA alter TLR-induced innate immune response

To study whether the metabolic environment modulates the innate immune response, we analyzed the impact of FA on TLR-mediated activation of mouse GM-CSF bone marrow-derived DC (GM-DC). In GM-DC, PA, a common saturated FA in processed food diets, alone did not induce a significant expression of pro-inflammatory cytokines, but it greatly modified *Il23a*, *Il6*, and *Il12a* expression in response to TLR activation (Figure 1A-B and S1A-C). Moreover, PA potentiated IL-23 expression induced by activation of another PRR Dectin-2 (by furfurman), but not by Dectin-1 (by curdlan), as well as by TNF, but not by IL-1β (Figure S1D). Likewise, PA robustly increased IL-23 expression upon TLR4 and TLR7/8 activation in bone marrow derived macrophages (BMDM) (Figure S1E). These data indicate that IL-23 expression is sensitive to the presence of a high FA metabolic environment.

Next, we focused on activation of DC with TLR7/8 ligand imiquimod (IMQ) which induced the strongest synergistic effects with PA. Interestingly, PA only modified expression of a subset of cytokines and chemokines among all induced by IMQ (Figure S1C), suggesting that FA promote a distinct innate immune signature in TLR-activated DC.

### PA modulates glycolysis in TLR-activated DC

TLR activation rapidly increases glycolysis in DC (Everts et al., 2014; Krawczyk et al., 2010) Furthermore, PA affects early TLR4 signaling in macrophages (Lancaster et al., 2018). Consequently, we hypothesized that PA might modulate the DC inflammatory response either by acting as a signaling molecule or by altering intracellular metabolism. Stimulation of GM-DC from wildtype and TLR4-deficient mice with IMQ and PA resulted in similar IL-23 induction (Figure S2A). Moreover, the up-regulation of IL-23 by PA was not due to NF-κB signaling (Figure S2B) or JNK siganling (Figure S2C-D). Furthermore, the monounsaturated oleic acid (OA) also increased IL-23 secretion upon IMQ activation, independently of TLR4 (Figure S2E). Taken together, these results show that FA increase IMQ-mediated IL-23 expression through a yet unknown mechanism. We thus investigated the impact of PA on intracellular metabolism in IMQ-stimulated DC. The dose-dependent increase of IL-23 expression and secretion upon IMQ and PA late co-stimulation was associated with a decrease of lactate secretion (Figure S2F), indicating reduced glycolytic activity. Moreover, PA suppressed lactate production during the late PRR activation (Figure 1C and S2G). Notably, PA presence did not affect extracellular acidification rate (ECAR), a surrogate measurement of glycolytic activity, and oxygen consumption rate (OCR), a measurement of oxidative phosphorylation (OXPHOS), during the immediate response to IMQ activation (Figure S2H-I). These results indicate that PA supresses late, but does not interfere with early steps of glycolytic reprogramming.

Next, we speculated that GM-DC become sensitive to metabolic effects of PA once the cells acquire “Warburg-like” metabolism (O’Neill and Pearce, 2016). Indeed, GM-DC demonstrated a highly glycolytic phenotype with inhibited mitochondrial respiration after IMQ activation (Figure 1F-I). Interestingly, while PA rapidly increased mitochondrial respiration in resting and IMQ-activated GM-DC (Figure 1F-G), only IMQ-activated “Warburg-like” cells displayed decreased glycolytic activity in response to PA (Figure 1H-I). Similarly, PA inhibited lactate secretion from TLR-activated “Warburg-like” BMDM (Figure S2J). Together, these data show that PA alters late stages of glycolytic reprogramming, resulting in a shift from aerobic glycolysis towards OXPHOS. This metabolic effect of PA was not due to alterations in glucose uptake (Figure S2K) or mitochondrial content (Figure S2L), nor was it explained by changes in activity of electron transport chain (ETC) complexes (Figure S2M). Although IMQ activation in GM-DC increased ATP levels and decreased ATP/ADP ratio (indicating elevated energy utilization), PA presence did not alter these parameters in IMQ-stimulated cells (Figure S2N).

**PA inhibits hexokinase activity and increases IL-23 expression independently of FAO**

Octanoic acid, a medium chain saturated FA, has been shown to inhibit key glycolytic enzymes in the liver (Weber et al., 1966). We hypothesized that PA might also inhibit glycolytic enzymes during the

late-stage TLR activation in GM-DC. Indeed, PA reversed the IMQ-induced increase of hexokinase (HK) activity at 24 hr (Figure 1J). Furthermore, various FA were capable to inhibit lactate secretion when added for 2 hr to GM-DC primed with IMQ for 24 hr (Figure S2O). Interestingly, 2-methyl-PA failed to inhibit lactate secretion in this setting, suggesting that an intact carboxylic acid moiety is required for the PA-dependent regulation of HK activity. Finally, the PA-mediated inhibition of HK was not due to its dissociation from mitochondrial outer membrane into the cytosol (Figure S2P).

We next assessed whether PA activation to PA-CoA was required for the inhibition of glycolytic activity. As the effect of PA on glycolysis was not modulated by triacsin C, an inhibitor of long-chain-FA-CoA ligases (Figure S2O and Q), its conversion to PA-CoA by these enzymes appears dispensable. Mitochondrial FAO depends on the activity of FA importers CPT1A and CPT2 (Mehta et al., 2017). *Cpt1a*-deficiency or silencing both *Cpt1a* and *Cpt2* did not alter the PA-mediated increase in IL-23 expression (Figure S3A-B and D-F). Moreover, *Cpt1a* deficiency did not affect the PA-mediated inhibition of HK activity in IMQ-activated GM-DC (Figure S3C). In addition, using a FAO-specific concentration of CPT1 inhibitor etomoxir (Divakaruni et al., 2018) did not alter IL-23 expression (Figure S3F). Furthermore, activation with IMQ decreased *Cpt1a* expression and reduced complete PA oxidation to $CO_2$ in GM-DC, despite a modest increase of acid-soluble metabolite (ASM) production, which was not rescued by pre-incubation with PA (Figure S3G-H), indicating greatly reduced PA catabolism. In line, IMQ activation led to elevated accumulation of free non-metabolized PA in GM-DC (Figure S3I). These results indicate that elevated intracellular FA concentrations, rather than their metabolization via FAO, are critical for the inhibition of HK activity and ensuing increase in IL-23 production at the late stage of TLR activation.

**PA inhibits glycolytic fluxes and disturbs mitochondrial fitness**

We next investigated whether the FAO-independent inhibition of glycolysis by PA was associated with alterations in the glycolytic pathway. IMQ-mediated DC activation induced the expression of genes encoding glycolytic enzymes and lactate transporters (Figure S4A and P left). Interestingly, PA addition to IMQ repressed *Ldha*, *Pfkl*, and *Pfkfb3* expression compared to IMQ alone (Figure S4A and P right). In line with gene expression data, [1,2-$^{13}$C]glucose flux via glycolysis into lactate (M+2) was significantly reduced upon PA treatment in IMQ activated GM-DC, whereas the (M+1) flux via the oxidative pentose phosphate pathway (PPP) was not altered (Figure 1K). Analysis of glycolysis intermediates showed non-significant increases of total fructose-1,6-biphosphate, 3-phosphoglycerate and pyruvate upon IMQ stimulation (Figure S4C-F). However, GM-DC co-stimulated with IMQ and PA displayed significantly decreased 3-phosphoglycerate compared to IMQ alone, in line with reduced glycolytic activity (Figure S4E and P).

IMQ activation generally down-regulated genes in the TCA cycle compared to resting cells (Figure S4G and P). These transcriptional changes led to accumulation of itaconate, and to elevated fumarate and malate levels, but no changes in citrate, isocitrate, and succinate were found in IMQ-activated GM-DC (Figure S4G-M and P). By contrast, IMQ and PA stimulation increased expression of pyruvate dehydrogenase (*Pdhb),* malate dehydrogenase (*Mdh1/2*) and mitochondrial isocitrate dehydrogenase 2 (*Idh2*) but decreased lactate dehydrogenase (*Ldha) expression* compared to IMQ-activation (Figure S4A, G & P). Surprisingly, in this setting, [1,2-$^{13}$C]glucose fluxes into TCA metabolites, such as isocitrate, itaconate, and malate, were significantly inhibited by PA (Figure 1L), and intracellular citrate and itaconate levels were reduced (Figure S4H and J). Itaconate regulates the late inflammatory response in macrophages (Bambouskova et al., 2018). Because PA decreased itaconate levels, we treated Acod1$^{-/-}$ (also known as Irg1$^{-/-}$) GM-DC, deficient in itaconate synthase, with IMQ and PA. While Irg1-deficiency affected IMQ+PA-induced IL-23 expression, the effect was relatively small (Figure S4Q). Thus, the up-regulation of IL-23 by PA is unlikely due to the modulation of intracellular itaconate.

Inhibited HK activity can lead to uncoupling of intra- from extramitochondrial metabolism (Robey and Hay, 2006), which might result in mitochondrial stress. Indicative of mitochondrial stress, mtROS generation was significantly increased by PA in IMQ-activated GM-DC (Figure 1M). Moreover, inhibition of HK activity by 2DG phenocopied the PA-induced increase of mtROS generation (Figure 1N). Taken together, these results indicate that the metabolic adaptation of glycolysis/ to a high FA environment is associated with inhibition of glycolysis, reduced glycolytic flux into the TCA cycle, and elevated mitochondrial stress.

**PA increases IL-23 expression through elevated generation of mtROS by complex I**

As PA elevated mitochondrial stress and increased IL-23 expression, we investigated whether these events are functionally associated by inhibiting of mtROS generation. Both mitoTEMPO, an mtROS scavenger, and rotenone, an inhibitor of ETC complex I, diminished mtROS generation and blunted the PA-dependent increase in IL-23 expression (Figure 2A-C). These results suggest that mtROS generation by complex I or III activity links FA to IL-23 expression. Notably, although it generally diminished mitochondrial respiration, mitoTEMPO neither prevented the PA-mediated inhibition of glycolytic and HK activities in IMQ-activated GM-DC nor altered GAPDH activity (Figure S5A-E). Thus, the increased mtROS generation is rather the result of inhibited glycolytic activity, not the cause.

ROS generation has been shown to rapidly up-regulate oxidative PPP activity in keratinocytes leading to increasing NADPH production to insure stabilization of redox balance and ROS clearance (Kuehne et al., 2015). We investigated whether alterations in PPP might functionally link the PA-mediated

glycolysis inhibition with increased mtROS production. PA inhibited activity of G6PDH, a rate limiting enzyme of the oxidative PPP, and treatment with mitoTEMPO diminished this effect (Figure S5F). In addition, the product of the oxidative PPP, ribose-5-phosphate (R5P), was decreased (Figure S5G), and [1,2-$^{13}$C]glucose fluxes into R5P via non-oxidative PPP (M+2), but not oxidative PPP (M+1), were decreased by PA in IMQ-activated GM-DC (Figure S5H). Interestingly, PA treatment also affected the PPP metabolite sedoheptulose-7-phosphate (S7P) (Figure S5I-J). Altogether, these data show that extracellular FA establishes a new metabolic equilibrium involving a modulation of the PPP activity, redox balance and mtROS generation in TLR-activated DC.

**Increased mitochondrial activity potentiates IL-23 expression**

To demonstrate the relevance of these results *in vivo*, we used a mouse model of IMQ-induced skin inflammation (Fits et al., 2009), which shares some features with human psoriasis, an IL-23-dependent disease (Teng et al., 2015). IMQ treatment and high-fat diet (HFD) feeding increased concentrations of non-esterified FA (NEFA) in plasma (Figure S6A-B) in agreement with published results (Stelzner et al., 2016). As reported (Kanemaru et al., 2015), HFD feeding increased epidermal thickening (Figure S6C-D). Moreover, in IMQ-treated mice, HFD feeding increased the population of IL-23$^{+}$ conventional DC (cDC) in skin draining inguinal lymph nodes (iLN) (Figure 2D). Upon HFD feeding, IMQ-activated cDC exhibited increased expression of genes involved in OXPHOS (Figure S6E) and generated more mtROS (Figure S6F), similar to the *in vitro* findings (Figure 1M). Notably, HFD feeding enhanced the IL-23-induced expression of a subset of IMQ-responsive genes in skin (Suárez-Fariñas et al., 2013), while it did not exert such an effect in the absence of IMQ (Figure S6G), suggesting that increased IL-23 production links HFD feeding with exacerbated skin pathology. Indeed, IMQ-induced skin inflammation was abrogated upon treatment with an IL-23-blocking antibody (Figure S6H). Moreover, in HFD fed mice treated with IMQ, Cpt1a-deficiency in cDC did not alter IL-23 expression and skin pathology (Figure S6I-K), in agreement with *in vitro* data (Figure S3B). Taken together, these results indicate that IMQ-activated cDC respond to a high FA environment *in vivo* via a FAO-independent mechanism by increasing mtROS generation and IL-23 expression. Next, we tested whether inhibition of ETC complex I activity could mitigate the effects of HFD feeding on increased IL-23 production *in vivo*. Metformin, a complex I inhibitor active in macrophages (Kelly et al., 2015), significantly reduced mitochondrial respiration in IMQ-activated GM-DC in the presence of PA (Figure S6L) and decreased IL-23 expression induced by IMQ and PA (Figure 2E) through an AMPK-independent mechanism (Figure S6M). In HFD-fed mice, metformin significantly reduced IL-23$^{+}$ cDC numbers in iLN and epidermal thickness induced by epicutaneous application of IMQ (Figure 2F) and mitigated psoriasis-associated gene expression in the skin (Figure S6N). Thus, *in vivo* IL-23

production by cDC is enhanced by HFD-derived NEFA through a mechanism dependent on complex I activity.

**PA-mediated increase of IL-23 expression is associated with a decrease in the glutamate/glutathione axis**

We noticed, that the level of NADPH, a product of oxidative PPP, was decreased (Figure 2G) and $NADP^+$/NADPH ratio was increased by PA in IMQ-activated cells (Figure S5L). Decreased NADPH might thus explain the elevated mtROS generation in response to PA. Interestingly, mitoparaquat (mitoPQ), which increase mtROS generation, up-regulated IL-23 expression in non-activated GM-DC but failed to potentiate IL-23 expression in IMQ-activated cells (Figure 2H). Glutathione (GSH) is an important component of the cellular anti-oxidant system (Mailloux et al., 2013). IMQ treatment resulted in a robust increase of GSH levels during the late TLR7/8 response, but this effect was reversed in the presence of PA (Figure 2I). Metabolomic data analysis revealed a decrease of intracellular glutamine and glutamate levels in IMQ-activated GM-DC treated with PA (Figure 2J), which was associated with inhibited flux into glutamate from glycolysis but not from glutaminolysis (Figure 2K). As glutamate is a key component for GSH synthesis, reduced glutamate may also account for the decreased levels of GSH, and thereby elevated mtROS generation, in GM-DC treated with IMQ and PA.

To test whether glutamine plays a role in the regulation of IL-23, we deprived GM-DC from glutamine before activation with IMQ and found significantly increased IL-23 expression (Figure 2L). Similarly, silencing of *Gls* and *Gls2* (Figure 2M), genes encoding enzymes mediating glutaminolysis, decreased glutamate and GSH levels (Figure 2N-O) and also increased mtROS generation and IL-23 expression in IMQ-activated GM-DC (Figure 2P-R). These results show that the pro-inflammatory effect of PA depends, at least in part, upon the reprogramming of the glutamine/glutamate/GSH axis.

**Upper glycolysis inhibition promotes IL-23 expression**

Because PA inhibited HK activity, we determined whether glycolytic inhibition was sufficient *per se* to enhance IL-23 expression. Treatment with 2DG led to elevated IL-23 expression in GM-DC in synergy with IMQ activation (Figure 3A). In line, intraperitoneal injection of 2DG significantly increased the accumulation of $IL\text{-}23^+$ cDC in IMQ-treated mice (Figure 3B). Taken together, these results show that inhibition of HK activity promotes IL-23 expression in TLR7/8-activated DC *in vitro* and *in vivo*. PA inhibited aerobic glycolysis in part through transcriptional regulation with a pronounced effect on *Pfkfb3* gene (Figure S4A). PFKFB3 increases glycolysis in macrophages (Jiang et al., 2016). Upon activation by IMQ and PA IL-23 expression was significantly increased in *Pfkfb3*-knocked-down GM-DC (Figure 3C). We next evaluated whether lower glycolysis was critical for IL-23 expression.

Combined inactivation of *Pfkl* (liver-type phosphofructokinase 1) and *Pfkp* (6-phosphofructo-1-kinase) decreased lactate secretion in IMQ-activated DC (Figure S7). However, this inactivation failed to up-regulate IL-23 expression (Figure S6O), indicating that the activity of upper, but not lower, glycolysis is essential for the regulation of IL-23 expression.

We further confirmed the role of upper glycolysis on IL-23 regulation using a model of genetic inactivation of HIF1α, which controls glycolytic activity in myeloid cells (Corcoran and O'Neill, 2016). Accordingly, lactate secretion and HK activity were significantly decreased in IMQ-activated HIF1α-deficient GM-DC (Figure 3D-F), while mtROS generation was significantly elevated (Figure 3G). In line, IMQ-activated, but not resting, HIF1α-deficient GM-DC displayed increased IL-23 expression and secretion (Figure 3H). Similar results were observed in HIF1α-deficient GM-DC from $Hif1a^{Vav/Vav}$ mice and tamoxifen-treated $Hif1a^{fl/fl}$Rosa26CreER mice (data not shown). Finally, the increase of IL-23 expression in IMQ-activated HIF1α-deficient GM-DC was abrogated by inhibiting mtROS generation, but not pyruvate dehydrogenase kinase (PDK) activity (Figure 3I). Taken together, these results show that chemical or genetic inhibitions of upper glycolysis lead to increased mtROS generation and IL-23 expression.

**Metabolic adaptation to a high FA environment is associated with a distinct transcriptional program**

To get further insight into the mechanisms of metabolic adaptation of DC to a high FA environment, we performed microarray analysis of GM-DC activated by IMQ and PA. IMQ alone induced pronounced changes in the DC transcriptional program, whereas PA alone only modestly affected gene expression (Figure 4A). By contrast, combined PA and IMQ treatment resulted in robust alteration of the DC transcriptional program, significantly modulating the expression of 874 genes (594 up-regulated and 280 down-regulated) compared to GM-DC treated with IMQ alone (Figure 4A-B). Analysis of the 594 up-regulated genes revealed an enrichment in the UPR, IRE1α/XBP1 pathway, and N-linked glycosylation (Figure 4C), including up-regulated expression of multiple genes from the UPR and the integrated stress response pathways (Figure 4D). Similarly, transcriptomic analysis of cDC isolated from IMQ-treated mice showed that, compared to CD, HFD feeding led to an increase in the UPR gene signature (Figure 4E). Taken together, these results suggest that metabolic adaptation of IMQ-activated DC to a high FA environment induces a distinct transcriptional program associated with exacerbated UPR.

**PA potentiates the UPR in TLR-activated DC**

The UPR regulates immune homeostasis and responses in DC (Martinon et al., 2010; Osorio et al.,

2014; Tavernier et al., 2017). Thus, we further analyzed the impact of UPR alterations on IL-23 expression. While PA alone acted on a very restricted gene subset, compared to IMQ alone, PA and IMQ differentially altered the expression of genes involved in the UPR (Figure S7A). In particular, combined action of IMQ and PA resulted in an additional increase of protein and/or gene expression of *Hspa5* (encoding BIP), *Ddit3* (encoding CHOP), and the spliced form of Xbp1 (XBP1s), but not the cleaved form of ATF6 p50 (Figure 5A-B and S7B). Likewise, in sorted cDC, key UPR genes were differentially expressed in response to HFD feeding (Figure S7C). Notably, this was not associated with elevated expression of the UPR receptors PERK or IRE1$\alpha$ (Figure 5A and S7B). In line with these data, the accumulation of XBP1s protein was maximal after 24 hr of combined treatment with IMQ and PA (Figure S7D-E). Furthermore, PA potentiated UPR activation by TLR2, 3, and 4 in GM-DC (Figure 5B), indicating that this effect is not limited to TLR7/8 pathway. These results thus show that the late metabolic adaptation of TLR-activated DC to a high FA environment results in a synergistic induction of the UPR.

**PA-induced metabolic adaptations hyperactivate the UPR**

Next, we determined whether metabolic adaptations to PA directly potentiate TLR-mediated UPR activation. In GM-DC treated with IMQ and PA, complex I and mtROS inhibition decreased CHOP and XBP1s expression (Figure 5C-H). Furthermore, inhibition of glycolysis in IMQ-activated GM-DC resulted in an increase of *Ddit3* and *Xbp1s* expression (Figure 5I-J). Accordingly, *Ddit3* and *Xbp1s* expression were significantly increased in HIF1$\alpha$-deficient GM-DC that failed to increase glycolytic activity upon TLR-activation (Figure 5K-L). Importantly, Xbp1-deficiency neither affected glycolytic activity, nor altered mitochondrial respiration in IMQ-activated GM-DC (Figure S7F), indicating that the increased UPR is a consequence rather than a cause of the inhibited glycolytic activity driven by PA. Taken together, these results indicate that metabolic adaptations to PA control the UPR in TLR-activated DC.

**UPR increases IL-23 expression through the PERK/CHOP and IRE1$\alpha$/XBP1 pathways**

Tunicamycin, a direct activator of the UPR, significantly increased IL-23 expression in resting GM-DC (Figure 6A). Interestingly, it synergistically enhanced IL-23 expression in IMQ-activated GM-DC (Figure 6A-B). Specific inhibitors of IRE1$\alpha$-dependent splicing activity and PERK signaling resulted in a significant and additive decrease of IL-23 expression in GM-DC treated with IMQ and PA (Figure 6C-D). Because these inhibitors also significantly decreased *Xbp1s, Atf4*, and *Ddit3* expression (data not shown), downstream IRE1$\alpha$ and PERK targets, we evaluated the impact of these transcription factors on IL-23 expression. Atf4 silencing decreased IL-23 expression in GM-DC activated with IMQ and PA,

but not IMQ alone (Figure S7G). Likewise, CHOP-deficient Ddit3$^{-/-}$ GM-DC (Oyadomari et al., 2001) displayed a lower IL-23 expression compared to Ddit3$^{+/+}$ cells (Figure 6E-F). IL-23 expression was also decreased in XBP1-deficient Xbp1$^{CD11c/CD11c}$ GM-DC (Osorio et al., 2014; Cubillos-Ruiz et al., 2015; Tavernier et al., 2017) upon IMQ and PA activation (Figure 6G-H). Moreover, Ddit3$^{-/-}$Xbp1$^{CD11c/CD11c}$ GM-DC (Tavernier et al., 2017), deficient for both XBP1 and CHOP (Figure S7H), showed a further decrease in IL-23 expression (Figure 6G-H). Of note, in IMQ-activated GM-DC, *Il6* induction by PA was dependent on mtROS generation, and XBP1- and CHOP-deficiency significantly attenuated *Il6* expression (Figure S7I-J). Furthermore, in IMQ-activated GM-DC, single or combined XBP1- and CHOP-deficiency diminished IL-23 expression potentiated upon glycolysis inhibition by 2DG (Figure 6I-J). GM-DC activation by IMQ and PA lead to increased mitochondrial UPR (UPR$^{mt}$) (Wu et al., 2014), and diminished mitochondrial localization of ATF5, a master regulator of the UPR$^{mt}$ in mammals (Shpilka and Haynes, 2018) (Figure S7K-L). However, *Atf5* knock-down did not alter IL-23 expression in GM-DC (Figure S7M). Moreover, silencing *Atf3*, a transcription factor that controls the integrated stress response (Jiang et al., 2004), increased IL-23 expression in GM-DC activated with IMQ and PA (Figure S7N).

Finally, ChIP-qPCR analysis revealed that CHOP and XBP1 interact with the mouse *Il23a* gene promoter in GM-DC and their binding increased by treatment with IMQ and/or PA (Figure 6K). Together, these results indicate that the endoplasmic reticulum UPR (UPR$^{ER}$), rather than UPR$^{mt}$ or the ATF3-dependent pathway, links metabolic adaptation to elevated extracellular FA concentrations to IL-23 expression in DC.

**HFD-feeding exacerbates IMQ-mediated inflammation through DC-specific XBP1-dependent regulation of IL-23**

To assess the contribution of the UPR to exacerbation of inflammatory response by HFD feeding, we evaluated IMQ-induced skin inflammation in mice harboring DC-specific XBP1-deficiency (Osorio et al., 2014). Whereas the number and proportion of IL-23$^{+}$ and IL-6$^{+}$ cDC were not significantly lower in CD-fed Xbp1$^{CD11c/CD11c}$ mice compared to their Xbp1$^{fl/fl}$ littermates, XBP1-deficiency in cDC strongly prevented the increase in IL-23$^{+}$ and IL-6$^{+}$ cDC in response to HFD feeding in IMQ-treated mice (Figure 7A-D). Importantly, Xbp1$^{CD11c/CD11c}$ mice displayed ameliorated IMQ-induced psoriasis-like skin inflammationbut showed no obvious difference in skin morphology without IMQ treatment (Figure 7E-F). These results show that UPR activation in DC contributes to TLR-mediated IL-23-driven inflammation enhanced by a high FA environment.

**Discussion**

Here, we demonstrate that the UPR integrates the signal driven by metabolic adaptation of activated DC to a high FA environment into a specific inflammatory program, characterized by elevated expression of IL-23. Upon pathogen-mediated activation via PRRs, innate immune cells must meet the high energetic demand required for anti-infectious defenses while ensuring moderate ROS levels to preserve the host from cell damage. Hence, a trade-off exists between highly effective ATP synthesis by OXPHOS and excessive mtROS production. Here, we demonstrate that, in DC, glycolysis is sensitive to a high FA environment at the late stage of PRR activation. Mechanistically, this metabolic adaptation to excessive FA exposure is due to the inhibition of HK activity, resulting in metabolic stress, in a decrease of carbon fluxes from glycolysis into the TCA cycle and, ultimately, in decreased mitochondrial fitness. In turn, it increases mtROS generation and drives a distinct immune response associated with hyperactivation of the UPR. Increased IL-23 and IL-6 are hallmarks of this metabolically-driven inflammatory response, and their expression is controlled by XBP1 and CHOP. IL-23 and IL-6 are known targets of NF-κB signaling upon TLR activation (Matsusaka et al., 1993; Sheikh et al., 2010). However, in our model, regulation of IL-23 by PA was not due to elevated NF-κB signaling. We also excluded the involvement of the $UPR^{mt}$ and ATF3-dependent pathway in regulation of IL-23 by PA. Similarly, a recently described JNK-dependent modulation of the early TLR response by PA (Lancaster et al., 2018) did not explain the PA-dependent up-regulation of IL-23 expression. On the other hand, we found that the glutamine/glutamate/glutathione axis contributes, in addition to decreased NADPH levels, to elevated mtROS levels upon PA treatment and in turn to increased IL-23 expression. By contrast, our data show that itaconate is unlikely to be involved in the PA-mediated up-regulation of IL-23 expression. Further studies are however needed to better understand such integrated reprogramming mechanisms.

Different types of TLR ligands, myeloid cell origins and the microenvironment, as well as duration of activation, can lead to differential metabolic responses (Stienstra et al., 2017). LPS treatment rewires glycolysis and TCA cycle metabolism in macrophages (Jha et al., 2015). We found similar transcriptional and metabolic alterations in DC activated by IMQ alone, where accumulation of non-metabolized PA and inhibited FAO suggest that FA are likely diverted from OXPHOS to avoid activation of the ETC and generation of mtROS. It is also possible that triglyceride synthesis acts as a transient buffer for extracellular FA. However, excessive extracellular FA likely overwhelm this protective mechanism (Chitraju et al., 2017), inhibiting HK activity and resulting in a metabolic disequilibrium and up-regulation of IL-23 and IL-6.

FAO contributes to polarization of M2 macrophages (Huang et al., 2014) or tolerogenic DC (Malinarich et al., 2015; Zhao et al., 2018), at least in the absence of an acute inflammatory stimulus. Importantly, a recent study challenged the role of FAO in M2 macrophage polarization as widely used etomoxir

concentrations show multiple FAO-independent metabolic effects that are absent in genetic models of FAO deficiency (Divakaruni et al., 2018). In line, we found that the PA-mediated increase of IL-23 expression is FAO independent and rather due to direct FA-mediated inhibition of the upper glycolysis in DC. HK has been shown to be an innate immune receptor for bacterial peptidoglycan detection of and its activity controls a dialog between mitochondria and inflammasome (Wolf et al., 2016). PFKFB3 has been recently described as an important glycolytic activator controlling antiviral immune responses in macrophages (Jiang et al., 2016). Our results suggest that HK and PFKFB3 link the metabolic adaptation of glycolysis to high extracellular PA with inflammatory responses, including increased IL-23 expression. Given that glycolysis controls a specific inflammatory signature, manipulating its activity is a potential therapeutic approach to control innate inflammation.

Various TLR ligands and ROS are known UPR inducers (Grootjans et al., 2016; Martinon et al., 2010) and our data confirm these findings. Importantly, our results demonstrate a finely regulated cross-talk between the adaptation of glycolytic activity to the metabolic environment and the UPR in TLR-activated DC. Elevated glycolytic activity and reduced mtROS generation in TLR-activated DC are protective mechanisms that cells use to prevent excessive UPR activation upon inflammation. This hypothesis is in line with the observation that glucose utilization prevents UPR-induced neuronal damage during TLR3-induced and viral inflammation (Wang et al., 2016). The UPR has been shown to induce certain pro-inflammatory cytokines, such as IL-6, via NOD1/2 – another class of PRRs (Keestra-Gounder et al., 2016). Whether a similar cross-talk also plays a role in the integration of environmental metabolic signals with PRRs, other than TLRs and Dectin-2, remains to be investigated.

Different branches of the UPR are involved in the homeostasis and the control of immune responses in DC (Janssens et al., 2014; Osorio et al., 2014; Tavernier et al., 2017). XBP1 regulates transcription of IL-6 and TNF in mouse macrophages (Martinon et al., 2010) and IL-23 production in human DC in response to zymosan (Márquez et al., 2017), while CHOP increases IL-23 expression in human DC in response to LPS and tunicamycin (Goodall et al., 2010). However, whether these effects require metabolic adaptations has not been investigated.

Our results show that XBP1 and the UPR are potential therapeutic targets for IL-23-dependent inflammatory diseases. Interestingly, a recent study identified that activation of XBP1s by lipid peroxidation results in abnormal lipid accumulation in tumor-associated DC and inhibits their capacity to support anti-tumor T lymphocytes (Cubillos-Ruiz et al., 2015), suggesting that XBP1 provides a strong link between metabolic and immune functions in DC.

IL-23 is a cytokine associated to protective immunity against some pathogens *(*Aychek et al., 2015*)*. Moreover, IL-23 plays a role in autoimmune diseases including psoriasis, psoriatic arthritis, and

ankylosing spondylitis (Pfeifle et al., 2017; Teng et al., 2015). It is likely that the mechanism of metabolic adaptation reported here is relevant to psoriasis and other IL-23-dependent pathologies. During acute inflammation, elevated FA produced by lipolysis in adipose tissue (Rittig et al., 2016) may potentiate IL-23 and IL-6 production by DC, thereby promoting inflammatory effects against pathogens. The innate immune system may have evolved to utilize the UPR as a sensor of elevated FA that tunes acute inflammatory responses of DC to the metabolic milieu. However, excessive FA in obesity and upon feeding with a HFD may result in hyperactivation of the UPR in DC and chronically increased production of IL-23 and IL-6.

In conclusion, our results demonstrate that adaptation of the glycolysis/mtROS axis to a metabolic environment rich in FA and ensuing hyperactivation of the UPR represents a new regulatory mechanism of the innate immune response.

**Acknowledgements:** This work was supported in part by grants from ANR and European Union: EGID ANR-10-LABX-46 (to B.S. and D.D.), National Psoriasis Foundation (USA) Early Career Research Grant (to D.A.M.), EMBO Long Term Fellowship (to J.T.H.) and MRC grant (MR/M023230/1) (to E.A.). B.S. is recipient of an ERC advanced grant (ERC-2016-AdG-694717). We thank members of the Bart Staels lab for help with experiments, Jean-Claude Sirard (Institut Pasteur de Lille, France), Juan R. Cubillos-Ruiz and Laurie H. Glimcher (Weill Cornell Medical College, New York, USA) and, Eik Hoffmann (Institut Pasteur de Lille, France) for mice, Morten Danielsen and Lea Johnsen (MS-Omics Inc., Copenhagen, Denmark) for assistance with LC-MS and GC-MS.

**Author contributions:** D.A.M., J.T.H., D.S.S, E.A and D.D. designed the study, analyzed the data, and wrote the manuscript with input from the other authors. B.S. discussed the data and edited the manuscript. D.A.M., J.T.H., L.L., S.F., S.Q., M.L., C.B., S.L., A.B., D.S.S, E.A. and D.D. performed the experiments with assistance from J.W., L.P., O.M.C., H.D., C.G., A.M., C.D., A.N., A.B., S.P. and N.R. Important mice, reagents, experimental and data analysis techniques were provided by J.S.A., S.O., T.V.H., J.C., M.F., B.V., M.V., A.V., K.K., G.M., S.T., C.P., P.C., L.B. M.P.L. and S.J. [21] D.S.S., E.A. and B.S contributed equally to this work.

**Declaration of interests**

The authors declare no competing interests

## Figure Legends

**Figure 1. PA rewires inflammatory response and metabolism in TLR-activated DC.**

GM-DC were activated by TLR ligands during indicated time without (control) or with PA.

(**A-C**) *Il23a* expression (**A**), IL-23p19 secretion (**B**) and lactate secretion (**C**) at 24 hr.

(**D-E**) Lactate secretion and *Il23a* expression at indicated time after activation.

(**F-I**) GM-DC activated during 24 hr, followed by extracellular flux analysis. Mitochondrial respiration calculated as OCR (**F-G**), glycolysis activity calculated as ECAR (**H-I**), before and after PA administration. Oligo, oligomycin; FCCP, carbonyl cyanide-4-(trifluoromethoxy)phenylhydrazone; AA, antimycin A; Rot, rotenone; 2DG, 2-deoxyglucose.

(**J**) HK activity in GM-DC treated as in **D-E**.

(**K-L**) Fluxes from 1,2-$^{13}$C-glucose into intracellular lactate (**K**), isocitric, itaconic, and malic acids (**L**). .

(**M-N**) MitoSOX staining in GM-DC activated by IMQ with/without PA (**M**) or with/without 2DG (**N**).

n = 3-5 per group. Data are shown as mean ± SEM. *P < 0.05, **P < 0.01, ***P < 0.001 (unpaired Student's t test or one-way ANOVA with Bonferroni test). #P < 0.05 as compared to mock/control treated cells (one-way ANOVA with Bonferroni test). See also Figure S1-5.

**Figure 2. PA increases IL-23 through mitochondrial respiration and mtROS generation.**

GM-DC were activated by IMQ without (Control) or with PA in the presence of indicated inhibitors for 24 hr.

(**A-C**) MitoSOX staining (**A**), *Il23a* expression and IL-23p19 secretion (**B-C**) in the presence of mitoTEMPO or rotenone.

(**D**) Male mice were fed CD or HFD, abdominal skin was treated with IMQ or vehicle during 6 days. Proportion of IL-23$^+$ cDC in iLN. n = 4-6 mice per group.

(**E**) *Il23a* expression in GM-DC in response to metformin.

(**F**) Male mice were fed HFD with or without metformin supplementation of drinking water during 3 days followed by IMQ application to belly skin. Number of IL-23$^+$ cDC in iLN 18 hr after IMQ treatment and average epidermal thickness after 5 days of IMQ treatment. n = 6-8 mice per group.

(**G**) NADP$^+$ and NADPH levels in GM-DC activated by IMQ with/without PA for 2-24 hr.

(**H**) MitoSOX staining in GM-DC activated by IMQ with/without mitoParaquat (mitoPQ).

(**I**) Intracellular GSH in GM-DC treated as in Figure **1D**.

(**J**) Intracellular glutamine and glutamate.

(**K**) Carbon fluxes from 1,2-$^{13}$C-glucose and U-$^{13}$C-glutamine into intracellular glutamate.

(**L**) *Il23a* expression in GM-DC pre-incubated with or without 2 mM glutamine for 4 hr and treated with

IMQ for 24 hr.

(**M-R**) *Gls* and *Gls2* expression (**M**), intracellular glutamate (**N**) and GSH (**O**), mtROS levels (**P**) and *Il23a* expression (**R**) in GM-DC transfected with siRNA against *Gls* and *Gls2* or control siRNA and 48 hr later treated with IMQ in media containing glutamine for 24 hr.

n = 3-6 per group. Data are shown as mean ± SEM. *P < 0.05, **P < 0.01, ***P < 0.001 by unpaired Student's t test. See also Figure S4 and S6.

**Figure 3. Upper glycolysis decreases IL-23 expression.**

(**A**) *Il23a* expression and IL-23 protein secretion in GM-DC activated by IMQ and treated with 2DG.

(**B**) Number and proportion of IL-23$^+$ cDC in iLN in mice 18 hr after IMQ application to abdominal skin and intraperitoneal injection with PBS or 2DG. n = 4-8 mice per group.

(**C**) *Pfkfb3* and *Il23a* expression in GM-DC transfected with siRNA against *Pfkfb3* or control siRNA and 48 hr later treated with IMQ.

(**D-J**) *Hif1a*$^{fl/fl}$ and *Hif1a*$^{Tie2/Tie2}$ GM-DC treated with IMQ. Lactate secretion (**D**), ECAR (**E**), hexokinase activity (**F**), MitoSOX$^+$ staining (**G**).

(**H-I**) *Il23a* expression and IL-23 secretion in *Hif1a*$^{fl/fl}$, *Hif1a*$^{Vav/Vav}$, and *Hif1a*$^{Tie2/Tie2}$ GM-DC treated with IMQ in the presence of mitoTEMPO and DCA.

n = 3-5 per group. Data are shown as mean ± SEM. *P < 0.05, **P < 0.01, ***P < 0.001 (unpaired Student's t test or two-way ANOVA with Sidak *post-hoc* test). See also Figure S3-4.

**Figure 4. PA and HFD feeding alter transcription program and induce the UPR in IMQ-activated DC.**

(**A**) Principal component (PC) analysis of 15000 genes with maximal average expression in GM-DC.

(**B**) Volcano plot of differential gene expression in GM-DC treated with IMQ versus treated with IMQ plus PA; number of genes with fold-change > 1.5 and < 0.67 and adjusted P < 0.05 are shown.

(**C**) Gene set enrichment analysis (GSEA) of the 594 genes from **B** using the Reactome database.

(**D**) K-mean clustering of the 15000 genes.

(**E**) GSEA using the "Unfolded Protein Response (UPR)" pathway in cDC sorted from iLN from IMQ-treated mice fed CD or HFD (15000 genes with maximal average expression).

n = 4 in each group. See also Figure S6.

**Figure 5. PA enhances the UPR through mtROS generation and inhibition of glycolysis.**

(**A**) Representative Western blot analysis of the UPR proteins in GM-DC treated with IMQ and PA. TBP (TATA-binding protein) and β-tubulin were used as loading controls.

(**B**) *Hspa5*, *Ddit3*, and *Xbp1s* expression in GM-DC treated with various TLR ligands without PA (Control) or with PA.

(**C-D**) *Ddit3* expression (**C**) and CHOP analysis by Western blot (**D**) in GM-DC treated as in **A** in the presence of rotenone.

(**E**) *Xbp1s* expression in GM-DC treated as in **C**.

(**F**) Representative flow cytometric analysis of XBP1s-venus$^{+}$ GM-DC from ERAI mice treated as in **C**.

(**G-J**) *Ddit3* and *Xbp1s* expression in GM-DC treated as in **A** in the presence of mitoTEMPO or 2DG.

(**K-L**) *Ddit3* and *Xbp1s* expression in Hif1a$^{fl/fl}$ and Hif1a$^{Vav/Vav}$ GM-DC treated with IMQ.

n = 2-5 per group. Data are shown as mean ± SEM. *P < 0.05, **P < 0.01, ***P < 0.001 (unpaired Student's t test or one-way ANOVA with Bonferroni test). #P < 0.05 as compared to mock/control treated cells (one-way ANOVA with Bonferroni test). See also Figure S7.

**Figure 6. PA and 2DG increase IL-23 expression through CHOP and XBP1s**

(**A-B**) *Il23a* expression (**A**) and IL-23p19 secretion (**B**) by GM-DC activated by IMQ and treated with tunicamycin (TN).

(**C-D**) *Il23a* expression (**C**) and IL-23p19 secretion (**D**) by GM-DC activated by IMQ and PA and treated with 4μ8C (IRE1$\alpha$ inhibitor) and/or GSK2606414 (PERK inhibitor).

(**E-F**) *Il23a* expression (**E**) and IL-23p19 secretion (**F**) by Ddit3$^{+/+}$ and Ddit3$^{-/-}$ GM-DC activated by IMQ and PA.

(**G-J**) *Il23a* expression (**G** and **I**) and IL-23p19 secretion (**H** and **J**) by Xbp1$^{fl/fl}$, Xbp1$^{CD11c/CD11c}$, and Ddit3$^{-/-}$Xbp1$^{CD11c/CD11c}$ GM-DC activated by IMQ and PA or 2DG.

(**K**) Schematic map of potential CHOP and XBP1 binding sites within the 5'-region of *Il23a* mouse gene and ChIP-qPCR analysis of XBP1 and CHOP binding to these sites in GM-DC treated as in (**C-D**). Data are shown as % DNA input enrichment for each site. TSS – transcription start site.

n = 3-5 per group. Data are shown as mean ± SEM. *P < 0.05, **P < 0.01, ***P < 0.001 (unpaired Student's t test or one-way ANOVA with Bonferroni test). See also Figure S7.

**Figure 7. HFD feeding exacerbates psoriasis-like inflammation through the Xbp1-dependent increase of IL-23 expression in cDC**

Xbp1$^{fl/fl}$ and Xbp1$^{CD11c/CD11c}$ littermate male mice were untreated or daily treated by application of IMQ to shaved abdominal skin during 5 days and fed CD or HFD.

(**A-D**) Number and proportion of IL-23$^{+}$ (**A-B**) and IL-6$^{+}$ (**C-D**) cDC in iLN.

(**E**) Representative MGG staining of sections from abdominal skin. Scale bar 50 μm.

(**F**) Average epidermal thickness of abdominal skin.

n = 6-8 mice per group (IMQ treated) and n = 2 mice per group (untreated). Data are shown as mean ± SEM. *P < 0.05, **P < 0.01, ***P < 0.001 (two-way ANOVA with Tukey's *post-hoc* test; significance of genotype and diet effects or their interaction is shown). See also Figure S7.

**Supplementary Figures Legends**

**Figure S1. PA alters expression of cytokines and chemokines in PRR-activated DC and macrophages. Related to Figure 1.**

(**A-B**) Expression of *Il6* and *Il12a* mRNAs in GM-DC activated by indicated TLR ligands during 24 hr in fatty acid-free medium (Control) or in the presence of PA. n = 3 per group. (**C**) Expression of cytokine and chemokine genes in GM-DC treated as in (**A-B**), analyzed by microarray. Data are shown as heat map with relative expression values (z-score). (**D**) Expression of *Il23a* mRNA in GM-DC treated with curdlan, furfurman, TNF or IL-1β in fatty acid-free medium (Control) or in the presence of PA for 24 hr. n = 4 per group. (**E**) Expression of *Il23a* mRNA in BMDC treated with IMQ or LPS in fatty acid-free medium (Control) or in the presence of PA for 24 hr. n = 4 per group. Data are shown as mean ± SEM. *P < 0.05, **P < 0.01, ***P < 0.001 (unpaired Student's t test).

**Figure S2. PA-mediated regulation of IL-23 expression in DC and macrophages. Related to Figure 1.**

(**A**) IL-23p19 secretion by $Tlr4^{+/+}$ and $Tlr4^{-/-}$ GM-DC activated by IMQ or LPS during 24 hr in the presence of 0.5 mM PA. n = 3~~-4~~ per group. (**B**) *Il23a* mRNA expression in GM-DC activated with IMQ and PA for 2 or 24 hr with/without NF-κB inhibitory peptide SN50. n = 3 per group. (**C**) WB analysis of JNK and p-JNK in GM-DC treated with IMQ and PA for 24 hr. n = 3 per group. (**D**) Mapk8, Mapk9, and Il23a mRNA expression in GM-DC transfected with siRNA against Mapk8 and Mapk9 and 48 hr later activated with IMQ and PA for 24 hr. n = 4 per group. (**E**) Il-23p19 secretion by GM-DC activated with IMQ in the presence of PA or OA for 24 hr. n = 4 per group. (**F**) *Il23a* mRNA expression, IL-23p19 secretion,~~ (D)~~ and lactate secretion by GM-DC activated by IMQ during 24 hr in fatty acid-free medium (Control) or in the presence of indicated concentrations of PA. n = 3 per group. (**G**) Lactate secretion from GM-DC treated as in Figure **S1D**. (**H-I**) Real time changes of ECAR (**H**) and OCR (**I**) measured by the extracellular flux analyzer in GM-DC incubated in fatty acid-free medium in the presence on glucose after administration of IMQ alone or IMQ plus PA. Time of injection of compounds during the test is indicated by arrow. n = 4 per group. (**J**) Lactate secretion from BMDM treated as in Figure **S1E**. (**K-L**) GM-DC activated by IMQ in fatty acid-free medium or in the presence of PA during 24 hr. Representative flow cytometric analysis of 2-NBDG uptake (**K**), mitochondrial content measured by staining with Mitotracker Green (**L**). Data from one of three reproducible independent experiments are shown. (**M**) Activity of electron transport chain complexes in permeabilized cells after addition of indicated substrates and inhibitors measured as oxygen consumptions by Oxygraph-2 k high-resolution respirometry in GM-DC activated by IMQ in fatty acid-free medium or in the presence of PA and/or etomoxir during 24 hr. n = 4 per group. (**N**) Relative ATP production and ATP/ADP ratio in GM-

DC activated by IMQ in fatty acid-free medium or in the presence of PA during 24 hr. n = 4 per group. (**O**) Hexokinase activity in GM-DC treated with IMQ for 24 hr and after that incubated with 0.5 mM of indicated FA for 2 hr. PA, palmitic acid (C16:0); 2Me-PA, 2-methylpalmitic acid (2Me-C16:0); OA, oleic acid (C18:1); LA, linoleic acid (C18:2); OCTA, octanoic acid (C8:0). n = 4 per group. (**P**) WB analysis of hexokinase 1 (HK1) protein in total cell lysates and isolated mitochondria and the cytosol from GM-DC activated with IMQ and PA fro 24 hr. n = 3 per group. (**Q**) ECAR in GM-DC activated with IMQ with/ without triacsin C for 24 hr and injected with BSA or PA during the “Seahorse” assay. n = 4 per group. Data are shown as mean ± SEM. *P < 0.05, **P < 0.01, ***P < 0.001 (unpaired Student’s t test or one-way ANOVA). NS – not significant.

**Figure S3. FAO-independent IL-23 expression in DC. Related to Figure 1.**

(**A-C**) Cpt1a (**A**), Il-23a (**B**) mRNAs expression, and HK activity (**C**) in $Cpt1a^{fl/fl}$ and $Cpt1a^{Itgax/Itgax}$ GM-DC activated with IMQ and PA for 24 hr. (**D-F**) Cpt1a (**D**), Cpt2 (**E**), and Il23a (**F**) mRNA expression GM-DC transfected with control siRNA or siRNAs against Cpt1a and Cpt2, treated with or without 3 μM etomoxir (Eto) and activated with IMQ and PA for 24 hr. (**G**) Cpt1a mRNA expression in BMDC activated with IMQ and PA for indicated time. (**H**) $^{14}CO_2$ production and accumulation of 14C in the acid-soluble metabolite fraction from GM-DC treated with IMQ and PA for 20 hr and incubated with $^{14}$C-PA for consecutive 4 hr. (**Il**) Relative abundance of intracellular PA measured by GC-MS in GM-DC treated treated with or without IMQ for 20 hr and incubated with PA for consecutive 4 hr. n = 3-6 per group. Data are shown as mean ± SEM. *P<0.05, **P<0.01, ***P<0.001 by t-test.

**Figure S4. Interaction between IMQ and PA results in rewiring of glycolysis and TCA cycle metabolism in DC. Related to Figures 1-3.**

(**A-O**) GM-DC activated by IMQ in fatty acid-free medium or in the presence of PA during 24 hr. Relative expression of genes controlling glycolysis (**A**) and TCA cycle metabolism (**G**) analyzed by microarray. Relative abundance of metabolites implicated in glycolysis (**B-F**) and TCA cycle (**H-O**) measured by LC-MS and GC-MS. (**P**) Schematic diagrams of gene and metabolite alterations in GM-DC activated by IMQ with/without PA. Up-regulated genes/metabolites are shown as red, down-regulated – blue. G6P, glucose 6-phosphate; F6P, fructose 6-phosphate; R5P, ribose 5-phosphate; S7P, sedoheptulose 7-phosphate; F1,6BP, fructose 1,6-bisphosphate; G3P, glyceraldehyde 3-phosphate; 1,3BPG, 1,3-bisphosphoglyceric acid; 3PG, 3-phosphoglyceric acid; 2PG, 2-phosphoglyceric acid; PEP, phosphoenolpyruvic acid. Results from n = 4-6 per group. (**Q**) Il23a mRNA expression in Acod1+/+ and Acod1−/− GM-DC treated with IMQ and PA for 24 hr. n = 4 per group. Data are shown as mean ± SEM. *P < 0.05, **P < 0.01, ***P < 0.001 (unpaired Student’s t test).

**Figure S5. Effects of PA to glycolysis and the PPP in DC. Related to Figure 3.**

(**A-B**) ECAR (**A**) and OCR (**B**) in GM-DC activated by IMQ with/without mitoTEMPO for 24 hr and injected with PA during the "Seahorse" assay. n = 4 per group. (**C-F**) Lactate secretion (**C**), HK activity (**D**), GAPDH activity (**E**), G6PDH activity (**F**) in GM-DC activate by IMQ and PA with/without mitoTEMPO for 24 hr. n = 3-4 per group. (**G-K**) Relative level of ribose-5-phosphate (**G**), carbon flux from 1,2-$^{13}$C-glucose into ribose-5-phosphate (**H**), relative level of sedoheptulose-7-phosphate (**I**), carbon flux from 1,2-$^{13}$C-glucose into sedoheptulose-7-phosphate (**J**) and schematic representation of the flux (**I**) in GM-DC treated with IMQ and PA for 24 hr. n = 3-6 per group. (**L**) $NADP^+$/NADPH ratios in GM-DC treated with IMQ and PA for indicated time. n = 4 per group. Data are shown as mean ± SEM. *P < 0.05, **P < 0.01, ***P < 0.001 (unpaired Student's t test or one-way ANOVA).

**Figure S6. HFD feeding exacerbates psoriasis-like inflammation through accumulation of IL-23$^+$ cDC in iLN and increased IL-23 signaling in the skin. Related to Figures 2 & 4.**

(**A-G**) Male mice were treated daily by application of vehicle or IMQ to shaved abdominal skin during 5 days and fed CD or HFD. Schematic design of this experiment (**A**). Concentration of non-esterified fatty acids (NEFAs) in plasma after day 5 of treatment (**B**). Representative MGG staining of abdominal skin sections (scale bar 50 μm) (**C**). Average epidermal thickness of abdominal skin (**D**). GSEA of genes from KEGG OXPHOS pathway in cDC sorted from iLN and analyzed by microarray (**E**). Proportion of mitoSOX$^+$ cDC in iLN (**F**). Volcano plots with $\log_2$ fold change versus $\log_{10}$ P-value of all transcripts (GSE69750, gray dots), including 1288 significantly up-regulated transcripts after intradermal injection of IL-23 (GSE50400, fold change (FC) > 2, q-value < 0.05) (red dots). Numbers of up- and down-regulated among the 1288 transcripts, and statistical significance levels of up-regulation of this entire IL-23-dependent set of transcripts are shown (**G**). (**H**) Mice were treated daily by application of IMQ to shaved abdominal skin during 5 days, injected IP with 3 mg anti-IL-23p19 neutralizing antibody or control IgG at 1$^{st}$ and 4$^{th}$ days, and fed CD or HFD. Average epidermal thickness in abdominal skin. Data are pooled from two independent experiments and shown as mean ± SEM. n = 4-12 mice per group. (**I-K**) Irradiated C57BL/6 mice reconstituted with bone marrow from Cpt1a$^{+/+}$ or Cpt1a$^{Zbtb46/Zbtb46}$ mice and fed 6 weeks post-irradiation with CD or HFD and epicutaneously treated with vehicle- or IMQ-containing cream for 5 days. Macroscopic aspect of lesions and disease activity score (**I**). MGG staining of lesions (**J**). Numbers and per cent IL-23$^+$ cDC (**K**) in iLN. n = 2-8 mice per group. Data are shown as mean ± SEM or box plots with median ± first-third quartiles. (**L-M**) GM-DC treated with IMQ and PA in the presence or absence of metformin during 24 hr. Oxygen consumption rate (OCR) and mitochondrial respiration (**L**), *Prkaa1*, *Prkaa2, and Il23a* mRNA

expression and IL-23p19 protein secretion (**M**). (**N**) mRNA expression of indicated genes in the skin from mice treated as in Figure **2D**. n = 2-4 mice per group. (O) Pfkl, Pfkp, Il23a mRNA expression and lactate secretion in GM-DC transfected with siRNA against Pfkl and Pfkp or control siRNA and 48 hr later treated with IMQ and PA for 24 hr. n = 4 per group. Data are shown as mean ± SEM. *P < 0.05, **P < 0.01, ***P < 0.001 (unpaired Student's t test or two-way ANOVA with Tukey's *post-hoc* test). NS – not significant.

**Figure S7. PA increases the UPR in IMQ-activated DC. Related to Figures 5-7.**

(**A**) Heat-map with relative expression of genes from GO:0030968 "Endoplasmic reticulum unfolded protein response" analyzed by microarray analysis in GM-DC activated by IMQ in fatty acid-free medium or in the presence of PA during 24 hr. n = 4 per group. (**B**) Quantification of WB from Figure **5A**. n = 5 per group. (**C**) Heat-map with relative expression of genes implicated in the UPR analyzed by microarray analysis in cDC isolated from iLN from mice treated with IMQ and fed CD or HFD. n = 4 mice per group. (**D-E**) GM-DC differentiated from the ER stress activated indicator (ERAI) mice. Representative flow cytometric analysis (**D**) and proportion (**E**) of Xbp1s-venus$^{+}$ GM-DC treated with IMQ and PA during 24 hr. n = 2 per group. #P < 0.05 vs. control groups and *P < 0.05 vs. IMQ groups. (**F**) Glycolytic and mitochondrial activities in Xbp1$^{fl/fl}$ and Xbp1$^{CD11c/CD11c}$ GM-DC activated with IMQ for 24 hr. n = 5 per group. (**G**) Atf4 and Il23a mRNA expression in GM-DC transfected with siRNA against Atf4 or control siRNA and 48 hr later activated by IMQ and PA for 24 hr. n = 4 per group. (**H**) Xbp1$^{fl/fl}$, Xbp1$^{CD11c/CD11c}$, and Ddit3$^{-/-}$Xbp1$^{CD11c/CD11c}$ GM-DC activated by IMQ in fatty acid-free medium or in the presence of PA during 24 hr. Deletion-specific qPCR for *Xbp1* and *Ddit3* mRNA expression. n = 4 per group. (**I**) *Il6* mRNA expression in GM-DC activated by IMQ with or without PA during 24 hr in the presence of rotenone or mitoTEMPO. n = 5 per group. (**J**) *Il6* mRNA expression in Xbp1$^{fl/fl}$, Xbp1$^{CD11c/CD11c}$ and Ddit3$^{-/-}$Xbp1$^{CD11c/CD11c}$ GM-DC activated by IMQ with or without PA during 24 hr. n = 4 per group. (**K**) Expression of genes from the mitochondrial UPR transcriptional signature in GM-DC. (**L**) WB analysis and quantification of ATF5 in isolated mitochondria from GM-DC. n = 2 per group. (**M-N**) Il23a, Atf5, and Atf3 mRNA expression in GM-DC transfected with control siRNA or siRNAs against Atf5 or Atf3 and 48 hr later activated by IMQ and PA for 24 hr. n = 4 per group. Data are shown as mean ± SEM. ND – not detected.*P < 0.05, **P < 0.01, ***P < 0.001 (unpaired Student's t test), #P < 0.05 vs. PA groups (unpaired Student's t test).

**Supplemental Table Legends**

**Supplemental Table S1.** Sequences for primers used in RT–qPCR experiments. Related to Figures 1-3 & 5-6 and STAR Methods.

**Supplemental Table S2.** Sequences for primers used in ChIP–qPCR experiments. Related to Figure 6 and STAR Methods.

## STAR METHODS

### CONTACT FOR REAGENT AND RESOURCE SHARING

Further information and requests for resources and reagents should be directed to and will be fulfilled by the Lead Contact, David Dombrowicz (david.dombrowicz@pasteur-lille.fr).

### EXPERIMENTAL MODEL AND SUBJECT DETAILS

#### Mice

Wild-type male C57BL/6 mice (8 weeks of age) were purchased from Charles River Laboratories (France). $Tlr4^{-/-}$ mice were a gift from Jean-Claude Sirard (Inserm U1019, Institut Pasteur de Lille, France). $Acod1^{-/-}$ mice were a gift from Eik Hoffmann (CIIL, Institut Pasteur de Lille, France). $Prkaa1^{+/-}$ and $Prkaa1^{-/-}$ mice (Jørgensen et al., 2004) were from Institut Cochin, Université Paris Descartes, Paris, France. $Hif1a^{Vav/Vav}$ mice (Vukovic et al., 2016) and $Hif1a^{Tie2/Tie2}$ mice were from MRC Centre for Regenerative Medicine, University of Edinburgh, UK. $Hif1a^{fl/fl}$Rosa26CreER mice were from Department of Molecular Medicine and Gene Therapy, Lund Stem Cell Center, Sweden. $Ddit3^{-/-}$ mice (Oyadomari et al., 2001) were from Division of Molecular Biology, Institute for Genome Research, Tokushima University, Japan. $Xbp1^{CD11c/CD11c}$ mice (Cubillos-Ruiz et al., 2015; Osorio et al., 2014) were from VIB Center for Inflammation, Gent University, Belgium or Department of Medicine, and Weill Cornell Medical College, New York, USA. $Ddit3^{-/-}Xbp1^{CD11c/CD11c}$ mice (Tavernier et al., 2017) and ERAI Xbp1-venus reporter mice (Iwawaki et al., 2004) were from VIB Center for Inflammation, Gent University, Belgium. $Cpt1a^{CD11c/CD11c}$ mice (Divakaruni et al., 2018) were from Institute of Infection Immunology, Hannover, Germany. $Cpt1a^{Zbtb46/Zbtb46}$ mice were from William Harvey Research Institute, London, UK. Mice were maintained in pathogen-free environment (12:12 hr light/dark cycle, 21°C-24°C) at the Institut Pasteur de Lille. 8-12-week-old male mice were used for all experiments with *ad libitum* access to water and food. During the experiments, food and bedding was changed daily to prevent any accumulation of food in the cages. Mice were randomized into the different treatment and diet groups equilibrated for body weight and age. Mice were fed a control diet (CD, standard rodent chow, 5% kcal fat) or high fat diet (HFD, 60% kcal fat) for the indicated period of time. Mice with fight wounds at the skin were excluded from analyses. All experiments were performed following approval by the Ethics Committee for Animal Experimentation from Nord-Pas de Calais Region (CEEA75-n°01-2002R and APAFIS#7160-2017040313471173).

#### Cell culture

Bone marrow-derived dendritic cells differentiated in the presence of GM-CSF (GM-DC) were obtained

from femurs of WT, Tlr4$^{-/-}$, Prkaa1$^{+/-}$, Prkaa1$^{-/-}$, Hif1a$^{Tie2/Tie2}$ , Hif1a$^{Vav/Vav}$, Ddit3$^{-/-}$, Xbp1$^{CD11c/CD11c}$, Ddit3$^{-/-}$Xbp1$^{CD11c/CD11c}$, Cpt1a$^{CD11c/CD11c}$, and ERAI Xbp1-venus reporter mice (C57BL/6 background, 8-12 weeks of age), cultured in DMEM media containing 10% fetal calf serum (FCS), 10 µM 2-mercaptoethanol, 25 mM HEPES, 10 µg/ml gentamycin and 20 ng/ml GM-CSF. Medium was refreshed every 3 days. GM-DC were used for experiments on day 14$^{th}$ of culture (mature GM-DC expressed CD11c$^{+}$MHCII$^{+}$ in > 80-90% cells). Bone marrow-derived macrophages differentiated in the presence of M-CSF (BMDM) were obtained from femurs of WT mice (C57BL/6 background, 8 weeks of age), cultured in RPMI media containing 10% FCS, 10 µM 2-mercaptoethanol, 10 µg/ml gentamycin and 20 ng/ml M-CSF and used at day 6. Cell viability was tested by 7AAD or trypan blue assays and was between 70-90% of live cells depending on type of treatment.

**METHOD DETAILS**

**IMQ-induced psoriasis-like skin inflammation**

IMQ-induced psoriasis-like inflammation was induced as previously described (Fits et al., 2009). Mice were treated with a daily topical dose (62.5mg) of IMQ cream (Aldara 5%) or control “Lanette” cream, unless stated otherwise, on the shaved abdominal skin for 5 days and sacrificed 24 hr later. Mice were fed HFD or control chow diet for the treatment duration. In some experiments, mice were treated by metformin in drinking water (0.5g/l) (Lien et al., 2014), starting at 3 days before and during treatment with IMQ. At the time of sacrifice, skin samples were directly frozen in liquid $N_2$ for RNA isolation or fixed in Immunohistofix for histological analysis.

For bone marrow chimeras, 8 – 10 week old C57BL/6 male mice were gamma-irradiated twice with 5 Gy 3 hr apart. Mice were reconstituted 3 hr later by intravenous (i.v.) injection with marrow cells (3 $10^6$ cells) harvested from the femurs and tibias of Cpt1$^{aZbtb46/Zbtb46}$ mice and control Cpt1$^{+/+}$ WT littermates. Mice were maintained on acidified water containing Baytril (Enrofloxacin) during the critical 3-week reconstitution period. Six weeks after reconstitution, animals were fed a HFD or CD and psoriasis-like inflammation was induced by IMQ application as described.

**Isolation of cells from iLN**

Mouse iLN were mechanically homogenized, passed through 70 µm filter and centrifugated at 400 g for 10 min. Cell pellets were washed two times with cold PBS and used for cell sorting or flow cytometry. For IL-23p19 staining, cells were incubated in DMEM containing brefeldin A (1µg/ml) at +37°C, 5% $CO_2$ for 4 hr.

**Flow cytometry**

Cells were stained with Zombie UV viability reagent during 15 min at +20°C, washed two times with cold PBS + 0.5% BSA, incubated with Fc block and antibodies mentioned in the figure legends and the Key Resources Table in PBS + 0.5% BSA during 30 min at +4°C, washed two times with cold PBS + 0.5% BSA, fixed with 1% PFA and used for flow cytometry. Flow cytometry analyses were performed on BD LSRFortessa X-20 flow cytometer. Results were acquired with the Diva software and analyzed using FlowJo software. cDC were defined as $CD3^{-}CD19^{-}CD64^{-}Ly6G^{-}CD11c^{+}MHCII^{+}$ cells.

**Sorting of cDCs from iLN**

$CD3^{-}CD19^{-}CD64^{-}Ly6G^{-}CD11c^{+}MHCII^{+}$ DCs were sorted from mouse iLN using BD Influx Cell Sorter (BD Biosciences). 5-8 × $10^5$ sorted cDC were used for RNA isolation with Arcturus Picopure RNA isolation Kit.

**Activation of GM-DC**

GM-DC (5 × $10^5$ per ml) were incubated in DMEM containing 10% FCS, 2 mM L-glutamine, 4.5 g/L glucose, and 10 µg/ml gentamycin and treated with 100 ng/ml Pam3CSK4, 10 µg/ml Poly(I:C), 100 ng/ml LPS, and 3µg/ml Imiquimod,100 µg/ml curdlan, 1 µg/ml furfurman, 50 ng/ml TNF, 50 ng/ml IL-1β with or without PA or other FA conjugated with BSA (0.065-0.5mM, molar ratio PA:BSA 6:1, OA:BSA 6:1) in the presence of 3 µM etomoxir, 5 mM 2-deoxyglucose, 1 µM rotenone, 5 mM metformin, 0.5 mM MitoTEMPO, 10 µM 4µ8C, 2 µM GSK2606414, 1 µM tunicamycin, 100 µg/ml SN50, 5 mM dichloroacetate (DCA), 10 µM triacsin C, 10 µM or 20 µM MitoPQ as indicated in figure legends. Reagents were added to cells simultaneously with IMQ or LPS, unless stated otherwise. SN50, MitoTEMPO, GSK2606414, 4µ8C, etomoxir, triacsin C and DCA were added 1 hr before other reagents. GM-DC were activated during 24 hr unless otherwise indicated.

**siRNA transfection**

5 × $10^5$ GM-DC per biological replicate were transfected with siRNA using Mouse Dendritic Cell Nucleofector Kit and Nucleofector II/2b device according to manufacturer's instructions. Cells were incubated during 48 hr in DMEM + 10% FCS and treated with IMQ and PA as described in TLR activation of GM-DC. Used siRNAs are mentioned in the figure legends and the Key Resources Table.

**2-NBDG uptake**

5 × $10^5$ GM-DC per biological replicate were incubated in DMEM without glucose during 1 hr following by incubation in the presence of 0.1 mM 2-NBDG during 10 min, washed two times with PBS and analyzed by flow cytometry.

**Analysis of mitochondrial content**

$5 \times 10^5$ GM-DC per biological replicate were incubated in DMEM in the presence of 1 µM MitoTracker Green FM during 15 min, washed two times with PBS and analyzed by flow cytometry.

**Mitochondrial ROS production**

To detect mitochondrial ROS, $5 \times 10^5$ GM-DC or cells isolated from iLN per biological replicate were incubated with 5 µM MitoSOX Red mitochondrial superoxide indicator at 37°C for 20 min in DMEM, washed two times with PBS, stained with surface antibody if indicated, and then analyzed with flow cytometry.

**Mitochondrial respiration assay**

$4 \times 10^6$ GM-DC per biological replicate were placed into the O2K chambers (Oroboros Instruments) and filled with MiR05 as described on the Oroboros website (http://www.bioblast.at/index.php/MiR05). After digitonin permeabilization for 10 min, mitochondrial respiration was studied at 25°C by adding sequentially the following compounds: glutamate (10 mM) and malate (2 mM), ADP (2.5 mM), succinate (10 mM), rotenone (0.5 µM), antimycin A (2.5 µM), TMPD / Ascorbate (0.5 mM / 2 mM), cytochrome c (10 µM) and sodium azide (100 mM).

**Chromatin Immunoprecipitation (ChIP)**

$5 \times 10^6$ GM-DC per biological replicate were cross-linked with 1% PFA at room temperature for 10 min, lysed, nuclei were isolated and resuspended in 0.4 ml nuclear lysis buffer containing 0.5% SDS. Nuclei were sonicated using a Bioruptor (Diagenode) according to the manufacturer's protocol, and chromatin was immunoprecipitated with antibodies against CHOP, XBP-1, and control IgG overnight at 4°C, followed by 4 hr incubation in the presence of Protein A/G beads. After washing, bead-bound chromatin was subject to decrosslinking for 4 hr at 65°C. DNA was purified using Agencourt AMPure beads. Relative DNA enrichment was quantified and normalized to input DNA by qPCR using SYBR Green Master Mix. Primers used for ChIP are listed in Table S2.

**RNA isolation**

Total RNA was isolated from GM-DC using Trizol reagent. Total RNA from sorted cDC was isolated using RNeasy Micro Kit.

**Reverse transcription and real-time PCR**

500 ng of total RNA isolated from GM-DC was treated with DNAse I and used to generate cDNA with High-capacity cDNA reverse transcription kit. Gene expression was measured by SybrGreen based qPCR. Results were normalized to the housekeeping genes *Hprt1* and *Rpl4*, and the ΔΔ*C*t method was employed for all real-time PCR analyses. Primers used for real-time PCR are listed in Table S1.

**Microarray analysis**

200 ng RNA from GM-DC was amplified with GeneChip WT PLUS Reagent Kit, labeled with GeneChip WT Terminal Labeling Kit. 5 ng RNA from sorted cDC was amplified with Ovation Pico WTA Systems V2, labeled with GeneChip WT Terminal Labeling Kit. The resulting complementary RNAs were hybridized on the GeneChip Mouse Gene 2.0 ST Array (Affymetrix) according to the manufacturer's protocol. Microarray data were normalized by the Robust Multi-Average method (Irizarry et al., 2003) by using affy R package (Gautier et al., 2004). Transcripts associated with annotated genes were selected for analysis. The expression dataset was collapsed to gene levels using a max-median approach following selection of top 15000 genes with maximal average expression levels among all experimental groups using Phantasus. Differentially expressed genes were identified by using limma R package (Smyth, 2005), which uses an empirical Bayesian approach to estimate variances in moderated t tests. Raw P values were adjusted for multiple testing using the Benjamini–Hochberg procedure.

**Protein Analysis**

Whole cell lysate from $1 \times 10^6$ GM-DC was extracted using RIPA lysis buffer supplemented with complete protease inhibitor cocktail and PhosSTOP phosphotase inhibitors. Proteins were diluted in Nupage LDS sample buffer, heated at 65°C for 5 min, and loaded on 4–12% NuPAGE Bis-Tris Gel. Proteins were transferred to nitrocellulose membrane using iBlot 2 Transfer stacks and blotted with commercial antibodies mentioned in the figure legends and the Key Resources Table.

**Seahorse assays**

$2.5 \times 10^5$ GM-DC per well were seeded in a XF24 plate and analyzed in a Seahorse XFe24 Analyzer. Oxygen consumption rate (OCR) and extracellular acidification rate (ECAR) were measured in DMEM with 25 mM glucose and 2 mM glutamine with or without of 0.5 mM PA, before and after the sequential injection of 0.75 µM oligomycin, 1.5 µM FCCP, 1µM of rotenone/antimycin A, and 50 mM 2-deoxyglucose. Mixing, waiting, and measurement times were 4, 2, and 2 min (3, 1, and 1 min in some experiments), respectively. Measures were normalized by total protein. Basal and maximal respiration

values were calculated by subtraction of OCR value after treatment of cells with rotenone and antimycin A (which corresponds to non-mitochondrial respiration) from OCR values in cells treated with glucose or with oligomycin and FCCP, respectively. Glycolysis and glycolytic capacity values were calculated by subtraction of ECAR value after treatment of cells with 2-deoxyglucose (which corresponds to non-glycolytic acidification) from ECAR values in cells treated with glucose or with oligomycin, respectively.

**Measurement of fatty acid oxidation**

Fatty acid oxidation was measured as described previously (Haas et al., 2012). Briefly, $5 \times 10^5$ GM-DC per biological replicate were pre-treated for 21 hr with IMQ or IMQ + 500μM PA. Cells were then switched to oxidation media containing 1mM carnitine, 500 μM PA, and 1μCi/mL $^{14}$C-PA for 3 hr. Media was acidified with 70% perchloric acid and $CO_2$ was captured with 1N NaOH. Complete oxidation (captured $CO_2$) and incomplete oxidation (acid soluble metabolites, ASMs) were calculated by counting the NaOH and cleared, acidified media.

**Metabolomics**

Metabolite extraction of GM-DC was performed on 2.5 million per well using 70°C aqueous 70% ethanol as described previously (Jha et al., 2015). Prior to collection, cells were treated with BSA (control), 500μM PA, IMQ or IMQ + 500μM PA for 24 hours. At collection, cells were placed immediately on ice, the media was removed and cells were washed three times with ice-cold PBS to remove residual media. Intracellular metabolites were extracted twice with hot ethanol using 10μM norvaline as an internal control. For LCMS, samples where dried under nitrogen flow and reconstituted in a milliQ water/acetonitrile (1:1) mixture for injection using a UPLC Acquity (Waters) separation system coupled with a Xevo G2 ToF (Waters) as described (Paglia et al., 2012) with slight modification. Compounds were ionized using an electrospray ionization source in negative mode. Data processing was performed in MATLAB (Mathworks, Inc.) using a custom made in-house protocol. Compound identification was performed using both retention time of authentic standards and accurate mass with an accepted deviation of 0.005 Da. For GCMS, samples were derivatized with methyl chloroformate as described (Smart et al., 2010) with slight modifications. Analysis was performed using GC (7890B, Agilent) coupled to a quadropole detector (59977B, Agilent) and controlled by ChemStation software (Agilent). Raw data was converted to netCDF format using Chemstation (Agilent), before processing in Matlab R2014b (Mathworks, Inc.) using PARADISe software as described (Johnsen et al., 2017). In both cases, samples were randomized prior to injection. All MS sample processing and analysis were performed by MS-Omics, Inc. (Copenhagen, Denmark).

### Histology

Mouse skin samples were fixed in ImmunoHistoFix and embedded in ImmunoHistoWax at 37°C. 5µm sections were stained with May-Grünwald Giemsa for measurement of epidermal thickness by using a Nikon Eclipse Ti-E microscope with NIS-Elements imaging software. Average epidermal thickness was determined as a mean of 10 measures calculated for each skin sample. We did blind investigators during epidermal thickness measurement.

## QUANTIFICATION AND STATISTICAL ANALYSES

### Statistical analyses of biological data

Data are presented as mean ± SEM. We tested whether data were normally distributed by Shapiro-Wilk test and examined quantile-quantile plots. Levene's test was used to analyze homogeneity of variances. For a two-group comparison two-sided Student's *t*-test was used. For more than two groups data were analyzed by ANOVA, or two-way ANOVA, followed by Tukey's (when we compared each group with every other group) or Sidak (when we compared groups within separate time points in repeated measures ANOVA) *post-hoc* tests for multiple comparisons. In case of data showing differences compared to normal distribution we applied two-sided Mann-Whitney U-test. Statistical analyses were performed with Prism 6 or R software. $p < 0.05$ was considered to be statistically significant and is presented as * $p < 0.05$, ** $p < 0.01$, *** $p < 0.001$, or **** $p < 0.0001$.

## DATA AND SOFTWARE AVAILABILITY

The accession numbers for microarray datasets reported in this paper are publicly available at the NCBI Gene Expression Omnibus: GSE68750, GSE110962, and GSE110963.

### References

Aychek, T., Mildner, A., Yona, S., Kim, K.-W., Lampl, N., Reich-Zeliger, S., Boon, L., Yogev, N., Waisman, A., Cua, D.J., et al. (2015). IL-23-mediated mononuclear phagocyte crosstalk protects mice from *Citrobacter rodentium*-induced colon immunopathology. Nat. Commun. *6*, 6525.

Bambouskova, M., Gorvel, L., Lampropoulou, V., Sergushichev, A., Loginicheva, E., Johnson, K., Korenfeld, D., Mathyer, M.E., Kim, H., Huang, L.-H., et al. (2018). Electrophilic properties of itaconate and derivatives regulate the IκBζ–ATF3 inflammatory axis. Nature *556*, 501–504.

Chitraju, C., Mejhert, N., Haas, J.T., Diaz-Ramirez, L.G., Grueter, C.A., Imbriglio, J.E., Pinto, S., Koliwad, S.K., Walther, T.C., and Farese, R.V. (2017). Triglyceride Synthesis by DGAT1 Protects Adipocytes from Lipid-Induced

ER Stress during Lipolysis. Cell Metab. *26*, 407-418.e3.

Chovatiya, R., and Medzhitov, R. (2014). Stress, Inflammation, and Defense of Homeostasis. Mol. Cell *54*, 281–288.

Corcoran, S.E., and O'Neill, L.A.J. (2016). HIF1α and metabolic reprogramming in inflammation. J. Clin. Invest. *126*, 3699–3707.

Cubillos-Ruiz, J.R., Silberman, P.C., Rutkowski, M.R., Chopra, S., Perales-Puchalt, A., Song, M., Zhang, S., Bettigole, S.E., Gupta, D., Holcomb, K., et al. (2015). ER Stress Sensor XBP1 Controls Anti-tumor Immunity by Disrupting Dendritic Cell Homeostasis. Cell *161*, 1527–1538.

Divakaruni, A.S., Hsieh, W.Y., Minarrieta, L., Duong, T.N., Kim, K.K.O., Desousa, B.R., Andreyev, A.Y., Bowman, C.E., Caradonna, K., Dranka, B.P., et al. (2018). Etomoxir Inhibits Macrophage Polarization by Disrupting CoA Homeostasis. Cell Metab. *28*, 490-503.e7.

Duan, Y., L. Zeng, C. Zheng, B. Song, F. Li, X. Kong, and K. Xu. 2018. Inflammatory Links Between High Fat Diets and Diseases. *Front Immunol* 9:2649.

Everts, B., Amiel, E., Huang, S.C.-C., Smith, A.M., Chang, C.-H., Lam, W.Y., Redmann, V., Freitas, T.C., Blagih, J., van der Windt, G.J.W., et al. (2014). TLR-driven early glycolytic reprogramming via the kinases TBK1-IKKε supports the anabolic demands of dendritic cell activation. Nat. Immunol. *15*, 323–332.

Fits, L. van der, Mourits, S., Voerman, J.S.A., Kant, M., Boon, L., Laman, J.D., Cornelissen, F., Mus, A.-M., Florencia, E., Prens, E.P., et al. (2009). Imiquimod-Induced Psoriasis-Like Skin Inflammation in Mice Is Mediated via the IL-23/IL-17 Axis. J. Immunol. *182*, 5836–5845.

Fullerton, J.N., and Gilroy, D.W. (2016). Resolution of inflammation: a new therapeutic frontier. Nat. Rev. Drug Discov. *15*, nrd.2016.39.

Gaber, T., Strehl, C., and Buttgereit, F. (2017). Metabolic regulation of inflammation. Nat. Rev. Rheumatol. *13*, nrrheum.2017.37.

Gautier, L., Cope, L., Bolstad, B.M., and Irizarry, R.A. (2004). affy—analysis of Affymetrix GeneChip data at the probe level. Bioinformatics *20*, 307–315.

Goodall, J.C., Wu, C., Zhang, Y., McNeill, L., Ellis, L., Saudek, V., and Gaston, J.S.H. (2010). Endoplasmic reticulum stress-induced transcription factor, CHOP, is crucial for dendritic cell IL-23 expression. Proc. Natl. Acad. Sci. U. S. A. *107*, 17698–17703.

Grootjans, J., Kaser, A., Kaufman, R.J., and Blumberg, R.S. (2016). The unfolded protein response in immunity

and inflammation. Nat. Rev. Immunol. *16*, 469–484.

Haas, J.T., Miao, J., Chanda, D., Wang, Y., Zhao, E., Haas, M.E., Hirschey, M., Vaitheesvaran, B., Farese, R.V., Kurland, I.J., et al. (2012). Hepatic insulin signaling is required for obesity-dependent expression of SREBP-1c mRNA but not for feeding-dependent expression. Cell Metab. *15*, 873–884.

Hotamisligil, G.S. (2017). Inflammation, metaflammation and immunometabolic disorders. Nature *542*, 177–185.

Huang, S.C.-C., Everts, B., Ivanova, Y., O'Sullivan, D., Nascimento, M., Smith, A.M., Beatty, W., Love-Gregory, L., Lam, W.Y., O'Neill, C.M., et al. (2014). Cell-intrinsic lysosomal lipolysis is essential for alternative activation of macrophages. Nat. Immunol. *15*, 846–855.

Ip, W.K.E., Hoshi, N., Shouval, D.S., Snapper, S., and Medzhitov, R. (2017). Anti-inflammatory effect of IL-10 mediated by metabolic reprogramming of macrophages. Science *356*, 513–519.

Irizarry, R.A., Hobbs, B., Collin, F., Beazer-Barclay, Y.D., Antonellis, K.J., Scherf, U., and Speed, T.P. (2003). Exploration, normalization, and summaries of high density oligonucleotide array probe level data. Biostatistics *4*, 249–264.

Iwawaki, T., Akai, R., Kohno, K., and Miura, M. (2004). A transgenic mouse model for monitoring endoplasmic reticulum stress. Nat. Med. *10*, 98.

Janssens, S., Pulendran, B., and Lambrecht, B.N. (2014). Emerging functions of the unfolded protein response in immunity. Nat. Immunol. *15*, 910–919.

Jha, A.K., Huang, S.C.-C., Sergushichev, A., Lampropoulou, V., Ivanova, Y., Loginicheva, E., Chmielewski, K., Stewart, K.M., Ashall, J., Everts, B., et al. (2015). Network Integration of Parallel Metabolic and Transcriptional Data Reveals Metabolic Modules that Regulate Macrophage Polarization. Immunity *42*, 419–430.

Jiang, H., Shi, H., Sun, M., Wang, Y., Meng, Q., Guo, P., Cao, Y., Chen, J., Gao, X., Li, E., et al. (2016). PFKFB3-Driven Macrophage Glycolytic Metabolism Is a Crucial Component of Innate Antiviral Defense. J. Immunol. *197*, 2880–2890.

Jiang, H.-Y., Wek, S.A., McGrath, B.C., Lu, D., Hai, T., Harding, H.P., Wang, X., Ron, D., Cavener, D.R., and Wek, R.C. (2004). Activating Transcription Factor 3 Is Integral to the Eukaryotic Initiation Factor 2 Kinase Stress Response. Mol. Cell. Biol. *24*, 1365–1377.

Johnsen, L.G., Skou, P.B., Khakimov, B., and Bro, R. (2017). Gas chromatography - mass spectrometry data processing made easy. J. Chromatogr. A *1503*, 57–64.

Jørgensen, S.B., Viollet, B., Andreelli, F., Frøsig, C., Birk, J.B., Schjerling, P., Vaulont, S., Richter, E.A., and

Wojtaszewski, J.F.P. (2004). Knockout of the alpha2 but not alpha1 5'-AMP-activated protein kinase isoform abolishes 5-aminoimidazole-4-carboxamide-1-beta-4-ribofuranosidebut not contraction-induced glucose uptake in skeletal muscle. J. Biol. Chem. *279*, 1070–1079.

Kanemaru, K., Matsuyuki, A., Nakamura, Y., and Fukami, K. (2015). Obesity exacerbates imiquimod-induced psoriasis-like epidermal hyperplasia and interleukin-17 and interleukin-22 production in mice. Exp. Dermatol. *24*, 436–442.

Karpe, F., Dickmann, J.R., and Frayn, K.N. (2011). Fatty Acids, Obesity, and Insulin Resistance: Time for a Reevaluation. Diabetes *60*, 2441–2449.

Keestra-Gounder, A.M., Byndloss, M.X., Seyffert, N., Young, B.M., Chávez-Arroyo, A., Tsai, A.Y., Cevallos, S.A., Winter, M.G., Pham, O.H., Tiffany, C.R., et al. (2016). NOD1 and NOD2 signalling links ER stress with inflammation. Nature *532*, 394–397.

Kelly, B., Tannahill, G.M., Murphy, M.P., and O'Neill, L.A.J. (2015). Metformin Inhibits the Production of Reactive Oxygen Species from NADH:ubiquinone Oxidoreductase to Limit Induction of IL-1β, and Boosts IL-10 in LPS-activated Macrophages. J. Biol. Chem. jbc.M115.662114.

Krawczyk, C.M., Holowka, T., Sun, J., Blagih, J., Amiel, E., DeBerardinis, R.J., Cross, J.R., Jung, E., Thompson, C.B., Jones, R.G., et al. (2010). Toll-like receptor–induced changes in glycolytic metabolism regulate dendritic cell activation. Blood *115*, 4742–4749.

Kuehne, A., Emmert, H., Soehle, J., Winnefeld, M., Fischer, F., Wenck, H., Gallinat, S., Terstegen, L., Lucius, R., Hildebrand, J., et al. (2015). Acute Activation of Oxidative Pentose Phosphate Pathway as First-Line Response to Oxidative Stress in Human Skin Cells. Mol. Cell *59*, 359–371.

Lampropoulou, V., Sergushichev, A., Bambouskova, M., Nair, S., Vincent, E.E., Loginicheva, E., Cervantes-Barragan, L., Ma, X., Huang, S.C.-C., Griss, T., et al. (2016). Itaconate Links Inhibition of Succinate Dehydrogenase with Macrophage Metabolic Remodeling and Regulation of Inflammation. Cell Metab. *24*, 158–166.

Lancaster, G.I., Langley, K.G., Berglund, N.A., Kammoun, H.L., Reibe, S., Estevez, E., Weir, J., Mellett, N.A., Pernes, G., Conway, J.R.W., et al. (2018). Evidence that TLR4 Is Not a Receptor for Saturated Fatty Acids but Mediates Lipid-Induced Inflammation by Reprogramming Macrophage Metabolism. Cell Metab. *27*, 1096-1110.e5.

Lien, F., Berthier, A., Bouchaert, E., Gheeraert, C., Alexandre, J., Porez, G., Prawitt, J., Dehondt, H., Ploton, M., Colin, S., et al. (2014). Metformin interferes with bile acid homeostasis through AMPK-FXR crosstalk. J. Clin. Invest. *124*, 1037–1051.

Mailloux, R.J., McBride, S.L., and Harper, M.-E. (2013). Unearthing the secrets of mitochondrial ROS and glutathione in bioenergetics. Trends Biochem. Sci. *38*, 592–602.

Malinarich, F., Duan, K., Hamid, R.A., Bijin, A., Lin, W.X., Poidinger, M., Fairhurst, A.-M., and Connolly, J.E. (2015). High Mitochondrial Respiration and Glycolytic Capacity Represent a Metabolic Phenotype of Human Tolerogenic Dendritic Cells. J. Immunol. 1303316.

Márquez, S., Fernández, J.J., Terán-Cabanillas, E., Herrero, C., Alonso, S., Azogil, A., Montero, O., Iwawaki, T., Cubillos-Ruiz, J.R., Fernández, N., et al. (2017). Endoplasmic Reticulum Stress Sensor IRE1α Enhances IL-23 Expression by Human Dendritic Cells. Front. Immunol. *8*, 639.

Martinon, F., Chen, X., Lee, A.-H., and Glimcher, L.H. (2010). TLR activation of the transcription factor XBP1 regulates innate immune responses in macrophages. Nat. Immunol. *11*, 411–418.

Matsusaka, T., Fujikawa, K., Nishio, Y., Mukaida, N., Matsushima, K., Kishimoto, T., and Akira, S. (1993). Transcription factors NF-IL6 and NF-kappa B synergistically activate transcription of the inflammatory cytokines, interleukin 6 and interleukin 8. Proc. Natl. Acad. Sci. U. S. A. *90*, 10193–10197.

Medzhitov, R. (2001). Toll-like receptors and innate immunity. Nat. Rev. Immunol. *1*, nri35100529.

Mehta, M.M., Weinberg, S.E., and Chandel, N.S. (2017). Mitochondrial control of immunity: beyond ATP. Nat. Rev. Immunol. *17*, 608–620.

Mills, E.L., Kelly, B., Logan, A., Costa, A.S.H., Varma, M., Bryant, C.E., Tourlomousis, P., Däbritz, J.H.M., Gottlieb, E., Latorre, I., et al. (2016). Succinate Dehydrogenase Supports Metabolic Repurposing of Mitochondria to Drive Inflammatory Macrophages. Cell *167*, 457-470.e13.

Netea, M.G., Balkwill, F., Chonchol, M., Cominelli, F., Donath, M.Y., Giamarellos-Bourboulis, E.J., Golenbock, D., Gresnigt, M.S., Heneka, M.T., Hoffman, H.M., et al. (2017). A guiding map for inflammation. Nat. Immunol. *18*, 826–831.

O'Neill, L.A.J., and Pearce, E.J. (2016). Immunometabolism governs dendritic cell and macrophage function. J. Exp. Med. *213*, 15–23.

Osorio, F., Tavernier, S.J., Hoffmann, E., Saeys, Y., Martens, L., Vetters, J., Delrue, I., De Rycke, R., Parthoens, E., Pouliot, P., et al. (2014). The unfolded-protein-response sensor IRE-1α regulates the function of CD8α+ dendritic cells. Nat. Immunol. *15*, 248–257.

Oyadomari, S., Takeda, K., Takiguchi, M., Gotoh, T., Matsumoto, M., Wada, I., Akira, S., Araki, E., and Mori, M. (2001). Nitric oxide-induced apoptosis in pancreatic beta cells is mediated by the endoplasmic reticulum stress pathway. Proc. Natl. Acad. Sci. U. S. A. *98*, 10845–10850.

Paglia, G., Hrafnsdóttir, S., Magnúsdóttir, M., Fleming, R.M.T., Thorlacius, S., Palsson, B.Ø., and Thiele, I. (2012). Monitoring metabolites consumption and secretion in cultured cells using ultra-performance liquid chromatography quadrupole-time of flight mass spectrometry (UPLC-Q-ToF-MS). Anal. Bioanal. Chem. *402*, 1183–1198.

Pfeifle, R., Rothe, T., Ipseiz, N., Scherer, H.U., Culemann, S., Harre, U., Ackermann, J.A., Seefried, M., Kleyer, A., Uderhardt, S., et al. (2017). Regulation of autoantibody activity by the IL-23-TH17 axis determines the onset of autoimmune disease. Nat. Immunol. *18*, 104–113.

Rittig, N., Bach, E., Thomsen, H.H., Pedersen, S.B., Nielsen, T.S., Jørgensen, J.O., Jessen, N., and Møller, N. (2016). Regulation of Lipolysis and Adipose Tissue Signaling during Acute Endotoxin-Induced Inflammation: A Human Randomized Crossover Trial. PLOS ONE *11*, e0162167.

Robey, R.B., and Hay, N. (2006). Mitochondrial hexokinases, novel mediators of the antiapoptotic effects of growth factors and Akt. Oncogene *25*, 4683–4696.

Shadel, G.S., and Horvath, T.L. (2015). Mitochondrial ROS Signaling in Organismal Homeostasis. Cell *163*, 560–569.

Sheikh, S.Z., Matsuoka, K., Kobayashi, T., Li, F., Rubinas, T., and Plevy, S.E. (2010). Cutting edge: IFN-gamma is a negative regulator of IL-23 in murine macrophages and experimental colitis. J. Immunol. Baltim. Md 1950 *184*, 4069–4073.

Shpilka, T., and Haynes, C.M. (2018). The mitochondrial UPR: mechanisms, physiological functions and implications in ageing. Nat. Rev. Mol. Cell Biol. *19*, 109–120.

Smart, K.F., Aggio, R.B.M., Van Houtte, J.R., and Villas-Bôas, S.G. (2010). Analytical platform for metabolome analysis of microbial cells using methyl chloroformate derivatization followed by gas chromatography-mass spectrometry. Nat. Protoc. *5*, 1709–1729.

Smyth, G.K. (2005). limma: Linear Models for Microarray Data. SpringerLink 397–420.

Stelzner, K., Herbert, D., Popkova, Y., Lorz, A., Schiller, J., Gericke, M., Klöting, N., Blüher, M., Franz, S., Simon, J.C., et al. (2016). Free fatty acids sensitize dendritic cells to amplify TH1/TH17-immune responses. Eur. J. Immunol. *46*, 2043–2053.

Stienstra, R., Netea-Maier, R.T., Riksen, N.P., Joosten, L.A.B., and Netea, M.G. (2017). Specific and Complex Reprogramming of Cellular Metabolism in Myeloid Cells during Innate Immune Responses. Cell Metab. *26*, 142–156.

Suárez-Fariñas, M., Arbeit, R., Jiang, W., Ortenzio, F.S., Sullivan, T., and Krueger, J.G. (2013). Suppression of

Molecular Inflammatory Pathways by Toll-Like Receptor 7, 8, and 9 Antagonists in a Model of IL-23-Induced Skin Inflammation. PLOS ONE *8*, e84634.

Tannahill, G.M., Curtis, A.M., Adamik, J., Palsson-McDermott, E.M., McGettrick, A.F., Goel, G., Frezza, C., Bernard, N.J., Kelly, B., Foley, N.H., et al. (2013). Succinate is an inflammatory signal that induces IL-1β through HIF-1α. Nature *496*, 238–242.

Tavernier, S.J., Osorio, F., Vandersarren, L., Vetters, J., Vanlangenakker, N., Van Isterdael, G., Vergote, K., De Rycke, R., Parthoens, E., van de Laar, L., et al. (2017). Regulated IRE1-dependent mRNA decay sets the threshold for dendritic cell survival. Nat. Cell Biol. *19*, 698–710.

Teng, M.W.L., Bowman, E.P., McElwee, J.J., Smyth, M.J., Casanova, J.-L., Cooper, A.M., and Cua, D.J. (2015). IL-12 and IL-23 cytokines: from discovery to targeted therapies for immune-mediated inflammatory diseases. Nat. Med. *21*, 719–729.

Vukovic, M., Sepulveda, C., Subramani, C., Guitart, A.V., Mohr, J., Allen, L., Panagopoulou, T.I., Paris, J., Lawson, H., Villacreces, A., et al. (2016). Adult hematopoietic stem cells lacking Hif-1α self-renew normally. Blood *127*, 2841–2846.

Wang, A., Huen, S.C., Luan, H.H., Yu, S., Zhang, C., Gallezot, J.-D., Booth, C.J., and Medzhitov, R. (2016). Opposing Effects of Fasting Metabolism on Tissue Tolerance in Bacterial and Viral Inflammation. Cell *166*, 1512-1525.e12.

Weber, G., Convery, H.J., Lea, M.A., and Stamm, N.B. (1966). Feedback inhibition of key glycolytic enzymes in liver: action of free fatty acids. Science *154*, 1357–1360.

Weis, S., Carlos, A.R., Moita, M.R., Singh, S., Blankenhaus, B., Cardoso, S., Larsen, R., Rebelo, S., Schäuble, S., Del Barrio, L., et al. (2017). Metabolic Adaptation Establishes Disease Tolerance to Sepsis. Cell *169*, 1263-1275.e14.

Wolf, A.J., Reyes, C.N., Liang, W., Becker, C., Shimada, K., Wheeler, M.L., Cho, H.C., Popescu, N.I., Coggeshall, K.M., Arditi, M., et al. (2016). Hexokinase Is an Innate Immune Receptor for the Detection of Bacterial Peptidoglycan. Cell *166*, 624–636.

Wu, Y., Williams, E.G., Dubuis, S., Mottis, A., Jovaisaite, V., Houten, S.M., Argmann, C.A., Faridi, P., Wolski, W., Kutalik, Z., et al. (2014). Multilayered Genetic and Omics Dissection of Mitochondrial Activity in a Mouse Reference Population. Cell *158*, 1415–1430.

Zhao, F., Xiao, C., Evans, K.S., Theivanthiran, T., DeVito, N., Holtzhausen, A., Liu, J., Liu, X., Boczkowski, D., Nair, S., et al. (2018). Paracrine Wnt5a-β-Catenin Signaling Triggers a Metabolic Program that Drives Dendritic Cell Tolerization. Immunity *48*, 147-160.e7.

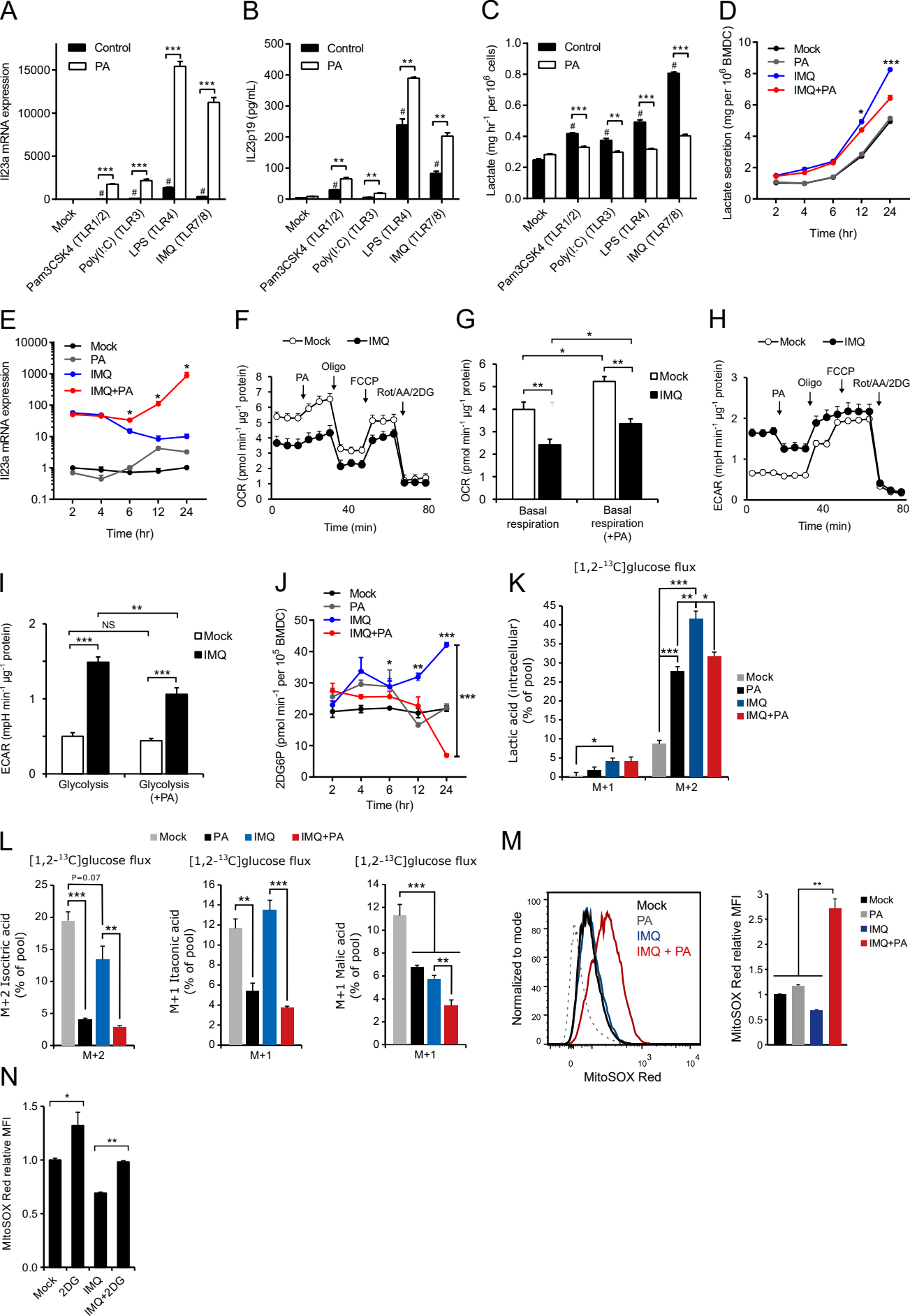
A
Control
PA
Il23a mRNA expression
Mock
Pam3CSK4 (TLR1/2)
Poly(I:C) (TLR3)
LPS (TLR4)
IMQ (TLR7/8)
B
IL23p19 (pg/mL)
C
Lactate (mg hr-1 per 10^6 cells)
D
Mock
PA
IMQ
IMQ+PA
Lactate secretion (mg per 10^6 BMDC)
Time (hr)
E
Il23a mRNA expression
Time (hr)
F
Mock
IMQ
PA
Oligo
FCCP
Rot/AA/2DG
OCR (pmol min-1 µg-1 protein)
Time (min)
G
Basal respiration
Basal respiration (+PA)
H
ECAR (mpH min-1 µg-1 protein)
I
NS
Glycolysis
Glycolysis (+PA)
J
2DG6P (pmol min-1 per 10^5 BMDC)
K
[1,2-13C]glucose flux
Lactic acid (intracellular) (% of pool)
M+1
M+2
L
P=0.07
M+2 Isocitric acid (% of pool)
M+1 Itaconic acid (% of pool)
M+1 Malic acid (% of pool)
M
Normalized to mode
MitoSOX Red
MitoSOX Red relative MFI
N
2DG
IMQ+2DG

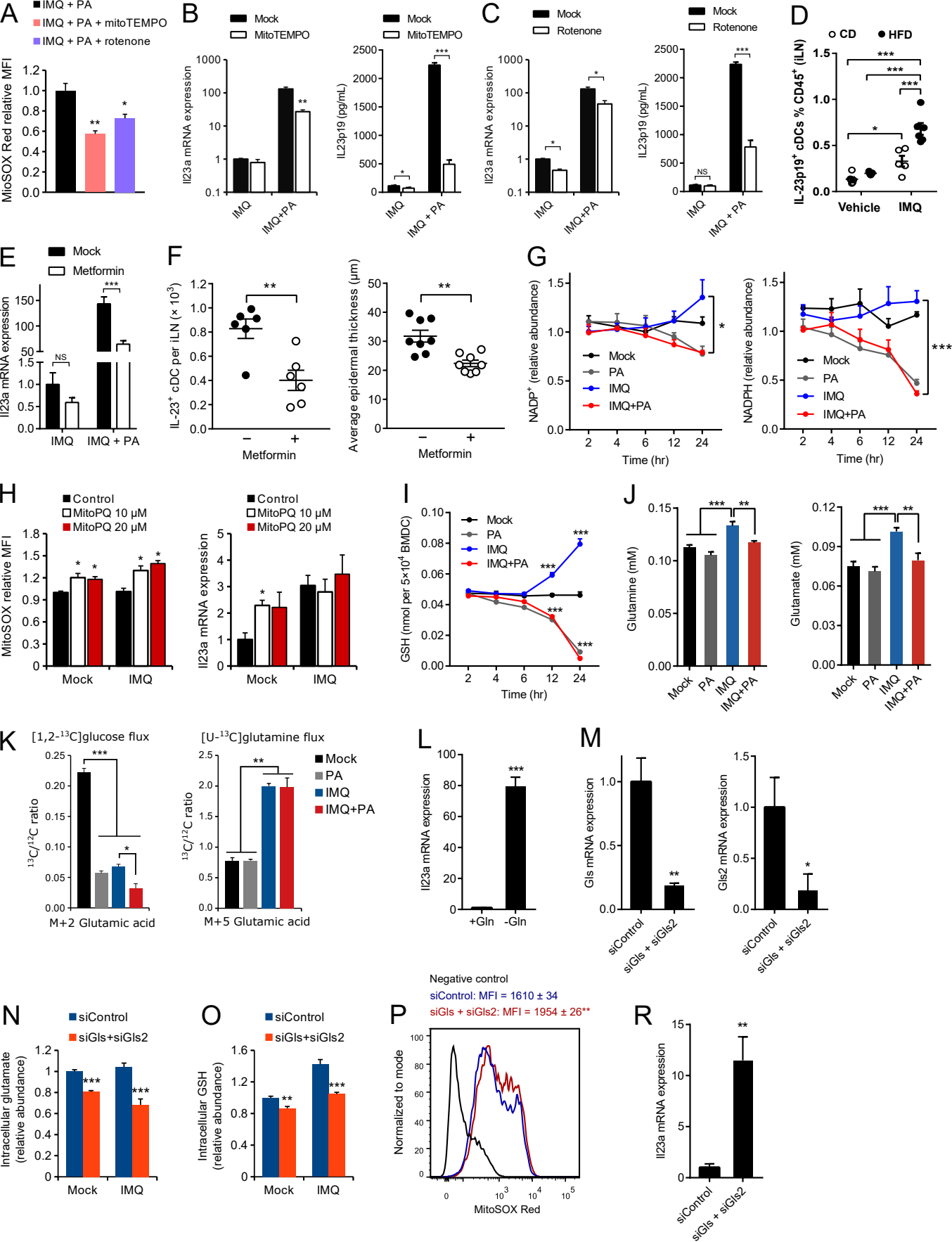
A
IMQ + PA
IMQ + PA + mitoTEMPO
IMQ + PA + rotenone
MioSOX Red relative MFI
B
Mock
MitoTEMPO
Il23a mRNA expression
IL23p19 (pg/mL)
IMQ
IMQ+PA
IMQ + PA
C
Mock
Rotenone
Il23a mRNA expression
IL23p19 (pg/mL)
NS
D
CD
HFD
IL-23p19+ cDCs % CD45+ (iLN)
Vehicle
IMQ
E
Mock
Metformin
Il23a mRNA expression
NS
IMQ
IMQ + PA
F
IL-23+ cDC per iLN (× 10^3)
Average epidermal thickness (μm)
Metformin
G
NADP+ (relative abundance)
NADPH (relative abundance)
Mock
PA
IMQ
IMQ+PA
Time (hr)
H
Control
MitoPQ 10 μM
MitoPQ 20 μM
MitoSOX relative MFI
Il23a mRNA expression
Mock
IMQ
I
Mock
PA
IMQ
IMQ+PA
GSH (nmol per 5×10^4 BMDC)
Time (hr)
J
Glutamine (mM)
Glutamate (mM)
Mock
PA
IMQ
IMQ+PA
K
[1,2-13C]glucose flux
[U-13C]glutamine flux
13C/12C ratio
M+2 Glutamic acid
M+5 Glutamic acid
Mock
PA
IMQ
IMQ+PA
L
Il23a mRNA expression
+Gln
-Gln
M
Gls mRNA expression
Gls2 mRNA expression
siControl
siGls + siGls2
N
siControl
siGls+siGls2
Intracellular glutamate (relative abundance)
Mock
IMQ
O
siControl
siGls+siGls2
Intracellular GSH (relative abundance)
Mock
IMQ
P
Negative control
siControl: MFI = 1610 ± 34
siGls + siGls2: MFI = 1954 ± 26**
Normalized to mode
MitoSOX Red
R
Il23a mRNA expression
siControl
siGls + siGls2

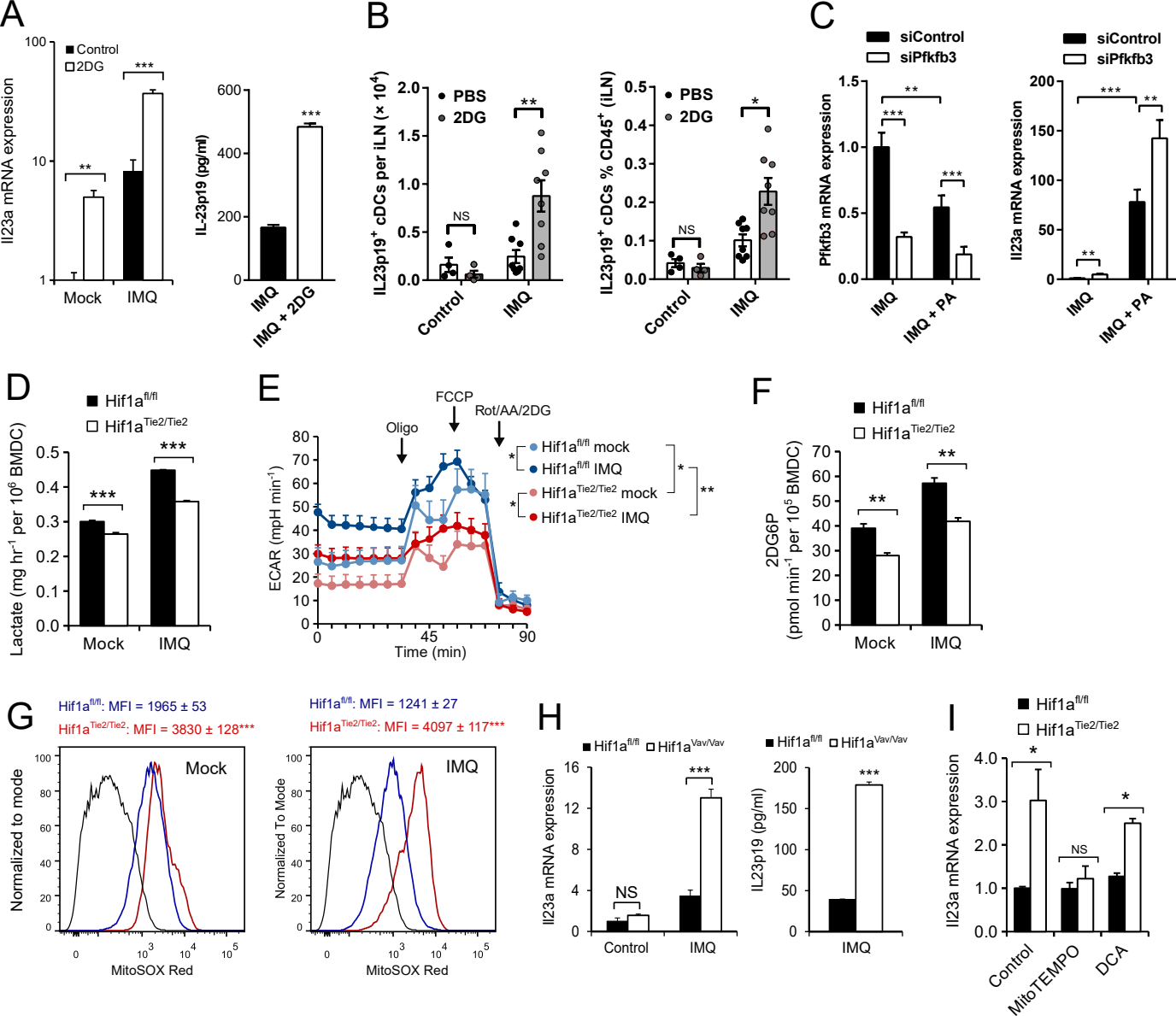
A
Control
2DG
Il23a mRNA expression
Mock
IMQ
IL-23p19 (pg/ml)
IMQ
IMQ + 2DG
B
PBS
2DG
IL23p19+ cDCs per iLN (× 10^4)
NS
Control
IMQ
IL23p19+ cDCs % CD45+ (iLN)
C
siControl
siPfkfb3
Pfkfb3 mRNA expression
IMQ
IMQ + PA
Il23a mRNA expression
D
Hif1a^fl/fl
Hif1a^Tie2/Tie2
Lactate (mg hr^-1 per 10^6 BMDC)
Mock
IMQ
E
FCCP
Oligo
Rot/AA/2DG
Hif1a^fl/fl mock
Hif1a^fl/fl IMQ
Hif1a^Tie2/Tie2 mock
Hif1a^Tie2/Tie2 IMQ
ECAR (mpH min^-1)
Time (min)
F
Hif1a^fl/fl
Hif1a^Tie2/Tie2
2DG6P (pmol min^-1 per 10^5 BMDC)
Mock
IMQ
G
Hif1a^fl/fl: MFI = 1965 ± 53
Hif1a^Tie2/Tie2: MFI = 3830 ± 128***
Hif1a^fl/fl: MFI = 1241 ± 27
Hif1a^Tie2/Tie2: MFI = 4097 ± 117***
Mock
IMQ
Normalized to mode
Normalized To Mode
MitoSOX Red
H
Hif1a^fl/fl
Hif1a^Vav/Vav
Il23a mRNA expression
Control
IMQ
IL23p19 (pg/ml)
I
Hif1a^fl/fl
Hif1a^Tie2/Tie2
Il23a mRNA expression
Control
MitoTEMPO
DCA

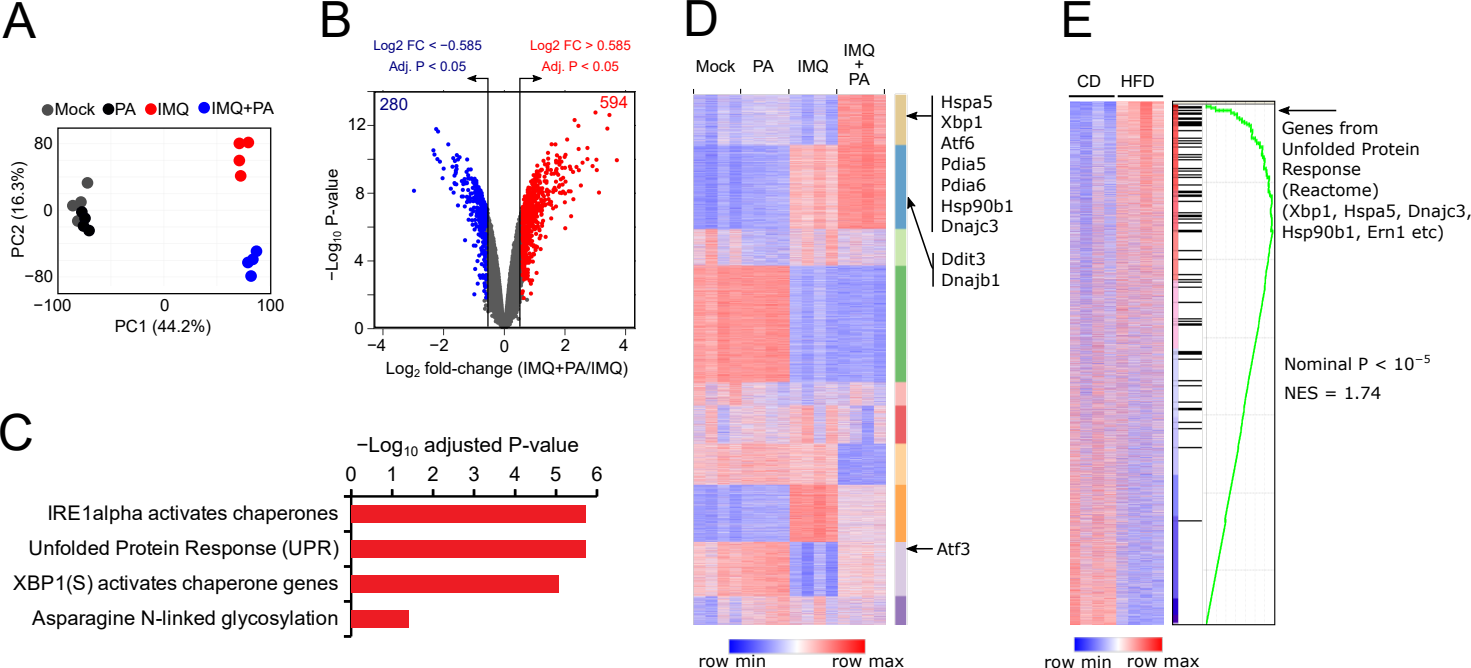
A
Mock
PA
IMQ
IMQ+PA
80
0
−80
PC2 (16.3%)
−100
0
100
PC1 (44.2%)
B
Log2 FC < −0.585
Adj. P < 0.05
Log2 FC > 0.585
Adj. P < 0.05
280
594
12
8
4
0
−Log10 P-value
−4
−2
0
2
4
Log2 fold-change (IMQ+PA/IMQ)
C
−Log10 adjusted P-value
0
1
2
3
4
5
6
IRE1alpha activates chaperones
Unfolded Protein Response (UPR)
XBP1(S) activates chaperone genes
Asparagine N-linked glycosylation
D
Mock
PA
IMQ
IMQ + PA
Hspa5
Xbp1
Atf6
Pdia5
Pdia6
Hsp90b1
Dnajc3
Ddit3
Dnajb1
Atf3
row min
row max
E
CD
HFD
Genes from Unfolded Protein Response (Reactome) (Xbp1, Hspa5, Dnajc3, Hsp90b1, Ern1 etc)
Nominal P < 10−5
NES = 1.74
row min
row max

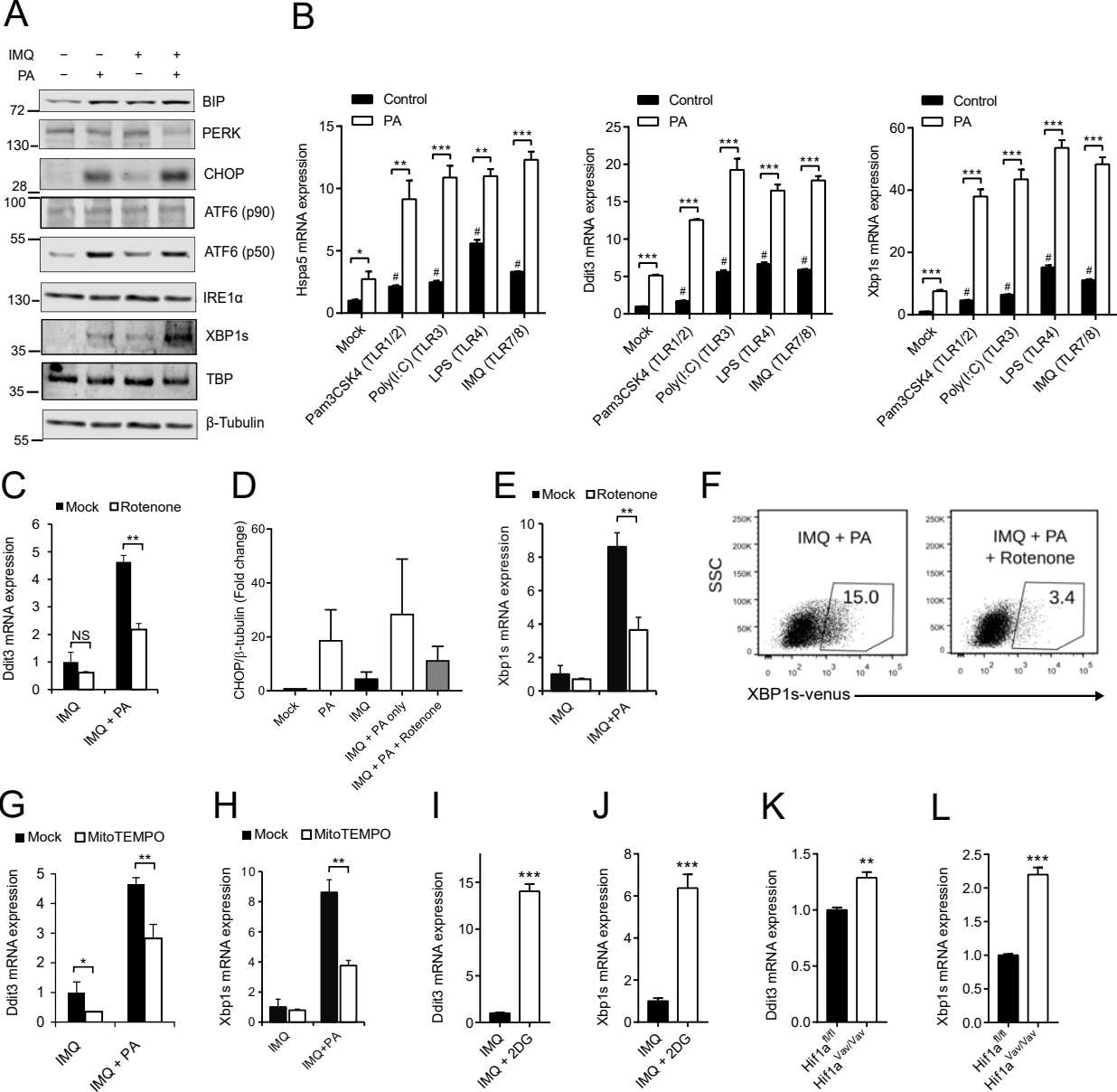
A
IMQ
PA
BIP
PERK
CHOP
ATF6 (p90)
ATF6 (p50)
IRE1α
XBP1s
TBP
β-Tubulin
72
130
28
100
55
130
35
35
55
B
Control
PA
Hspa5 mRNA expression
Ddit3 mRNA expression
Xbp1s mRNA expression
Mock
Pam3CSK4 (TLR1/2)
Poly(I:C) (TLR3)
LPS (TLR4)
IMQ (TLR7/8)
C
Mock
Rotenone
Ddit3 mRNA expression
NS
IMQ
IMQ + PA
D
CHOP/β-tubulin (Fold change)
Mock
PA
IMQ
IMQ + PA only
IMQ + PA + Rotenone
E
Mock
Rotenone
Xbp1s mRNA expression
IMQ
IMQ+PA
F
IMQ + PA
15.0
IMQ + PA
+ Rotenone
3.4
SSC
XBP1s-venus
G
Mock
MitoTEMPO
Ddit3 mRNA expression
IMQ
IMQ + PA
H
Mock
MitoTEMPO
Xbp1s mRNA expression
IMQ
IMQ+PA
I
Ddit3 mRNA expression
IMQ
IMQ + 2DG
J
Xbp1s mRNA expression
IMQ
IMQ + 2DG
K
Ddit3 mRNA expression
Hif1a fl/fl
Hif1a Vav/Vav
L
Xbp1s mRNA expression
Hif1a fl/fl
Hif1a Vav/Vav

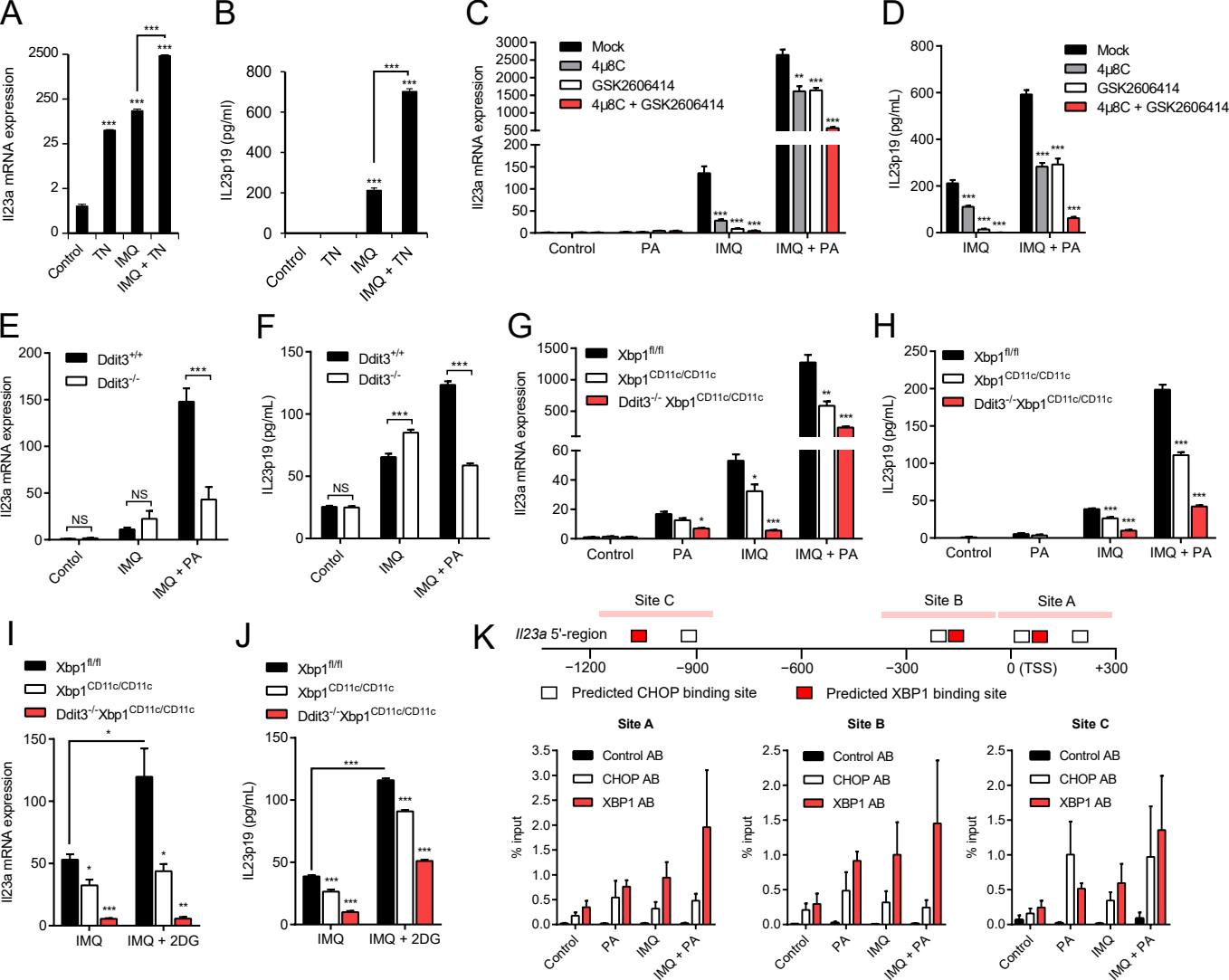
A
Il23a mRNA expression
Control
TN
IMQ
IMQ + TN
B
IL23p19 (pg/ml)
C
Il23a mRNA expression
Mock
4μ8C
GSK2606414
4μ8C + GSK2606414
Control
PA
IMQ
IMQ + PA
D
IL23p19 (pg/mL)
E
Il23a mRNA expression
Ddit3+/+
Ddit3-/-
NS
F
IL23p19 (pg/mL)
G
Il23a mRNA expression
Xbp1fl/fl
Xbp1CD11c/CD11c
Ddit3-/- Xbp1CD11c/CD11c
H
IL23p19 (pg/mL)
I
Il23a mRNA expression
IMQ + 2DG
J
IL23p19 (pg/mL)
K
Il23a 5'-region
Site C
Site B
Site A
−1200
−900
−600
−300
0 (TSS)
+300
Predicted CHOP binding site
Predicted XBP1 binding site
Site A
Site B
Site C
Control AB
CHOP AB
XBP1 AB
% input

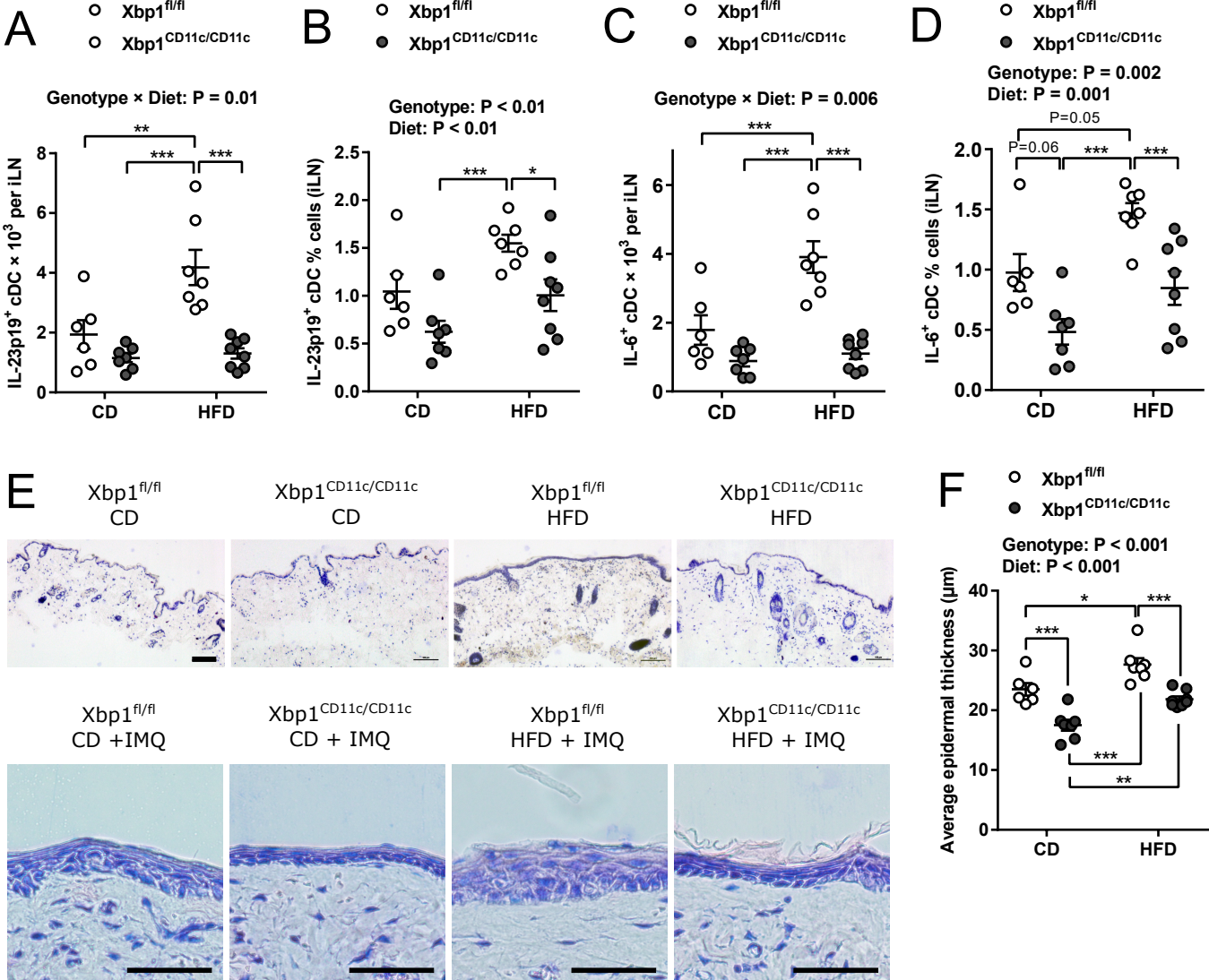
A
Xbp1fl/fl
Xbp1CD11c/CD11c
Genotype × Diet: P = 0.01
IL-23p19+ cDC × 10³ per iLN
CD
HFD
B
Xbp1fl/fl
Xbp1CD11c/CD11c
Genotype: P < 0.01
Diet: P < 0.01
IL-23p19+ cDC % cells (iLN)
CD
HFD
C
Xbp1fl/fl
Xbp1CD11c/CD11c
Genotype × Diet: P = 0.006
IL-6+ cDC × 10³ per iLN
CD
HFD
D
Xbp1fl/fl
Xbp1CD11c/CD11c
Genotype: P = 0.002
Diet: P = 0.001
P=0.05
P=0.06
IL-6+ cDC % cells (iLN)
CD
HFD
E
Xbp1fl/fl CD
Xbp1CD11c/CD11c CD
Xbp1fl/fl HFD
Xbp1CD11c/CD11c HFD
Xbp1fl/fl CD +IMQ
Xbp1CD11c/CD11c CD + IMQ
Xbp1fl/fl HFD + IMQ
Xbp1CD11c/CD11c HFD + IMQ
F
Xbp1fl/fl
Xbp1CD11c/CD11c
Genotype: P < 0.001
Diet: P < 0.001
Average epidermal thickness (µm)
CD
HFD

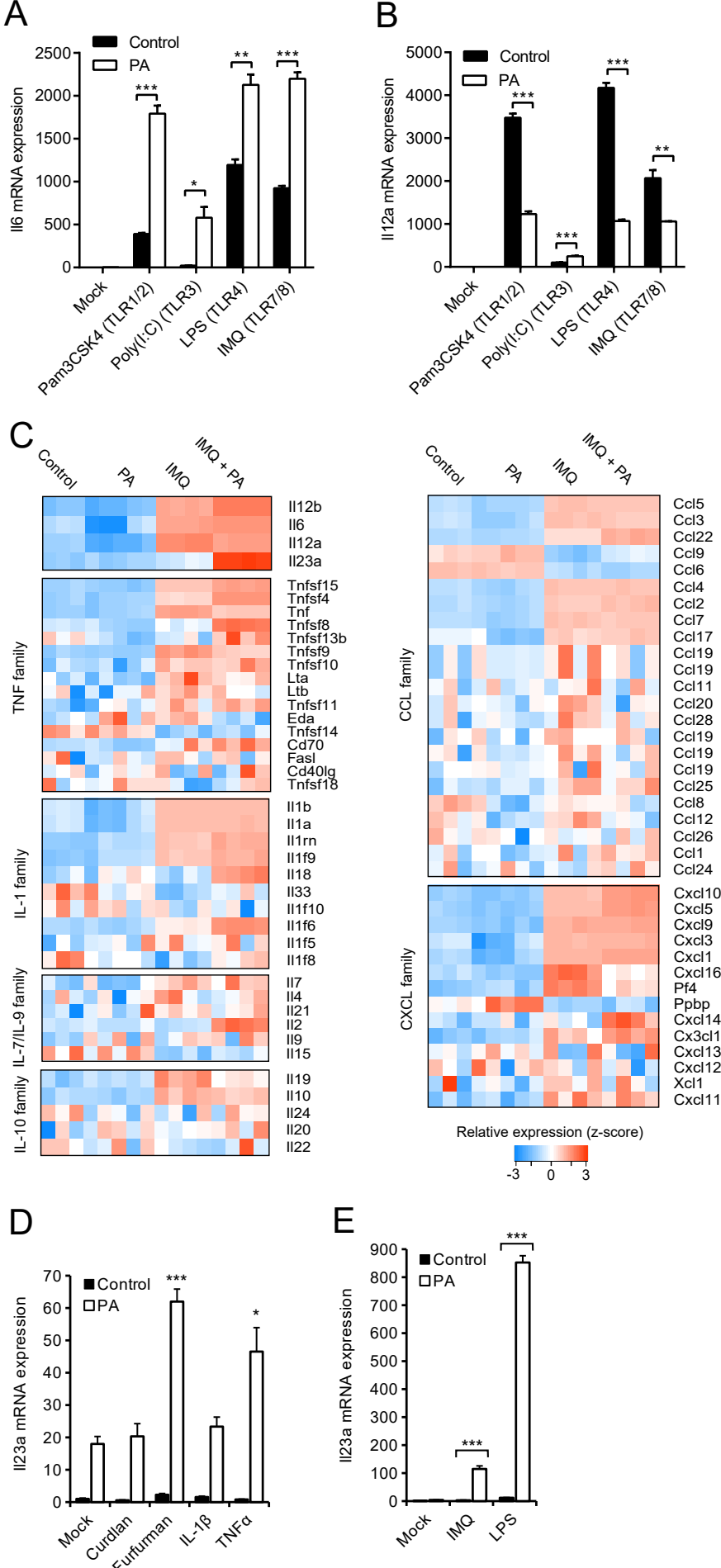
A
Control
PA
Il6 mRNA expression
2500
2000
1500
1000
500
0
***
*
**
***
Mock
Pam3CSK4 (TLR1/2)
Poly(I:C) (TLR3)
LPS (TLR4)
IMQ (TLR7/8)
B
Control
PA
Il12a mRNA expression
5000
4000
3000
2000
1000
0
***
***
***
**
Mock
Pam3CSK4 (TLR1/2)
Poly(I:C) (TLR3)
LPS (TLR4)
IMQ (TLR7/8)
C
Control
PA
IMQ
IMQ + PA
Il12b
Il6
Il12a
Il23a
TNF family
Tnfsf15
Tnfsf4
Tnf
Tnfsf8
Tnfsf13b
Tnfsf9
Tnfsf10
Lta
Ltb
Tnfsf11
Eda
Tnfsf14
Cd70
Fasl
Cd40lg
Tnfsf18
IL-1 family
Il1b
Il1a
Il1rn
Il1f9
Il18
Il33
Il1f10
Il1f6
Il1f5
Il1f8
IL-7/IL-9 family
Il7
Il4
Il21
Il2
Il9
Il15
IL-10 family
Il19
Il10
Il24
Il20
Il22
CCL family
Ccl5
Ccl3
Ccl22
Ccl9
Ccl6
Ccl4
Ccl2
Ccl7
Ccl17
Ccl19
Ccl19
Ccl11
Ccl20
Ccl28
Ccl19
Ccl19
Ccl19
Ccl25
Ccl8
Ccl12
Ccl26
Ccl1
Ccl24
CXCL family
Cxcl10
Cxcl5
Cxcl9
Cxcl3
Cxcl1
Cxcl16
Pf4
Ppbp
Cxcl14
Cx3cl1
Cxcl13
Cxcl12
Xcl1
Cxcl11
Relative expression (z-score)
-3
0
3
D
Control
PA
Il23a mRNA expression
70
60
50
40
30
20
10
0
***
*
Mock
Curdlan
Furfurman
IL-1β
TNFα
E
Control
PA
Il23a mRNA expression
900
800
700
600
500
400
300
200
100
0
***
***
Mock
IMQ
LPS

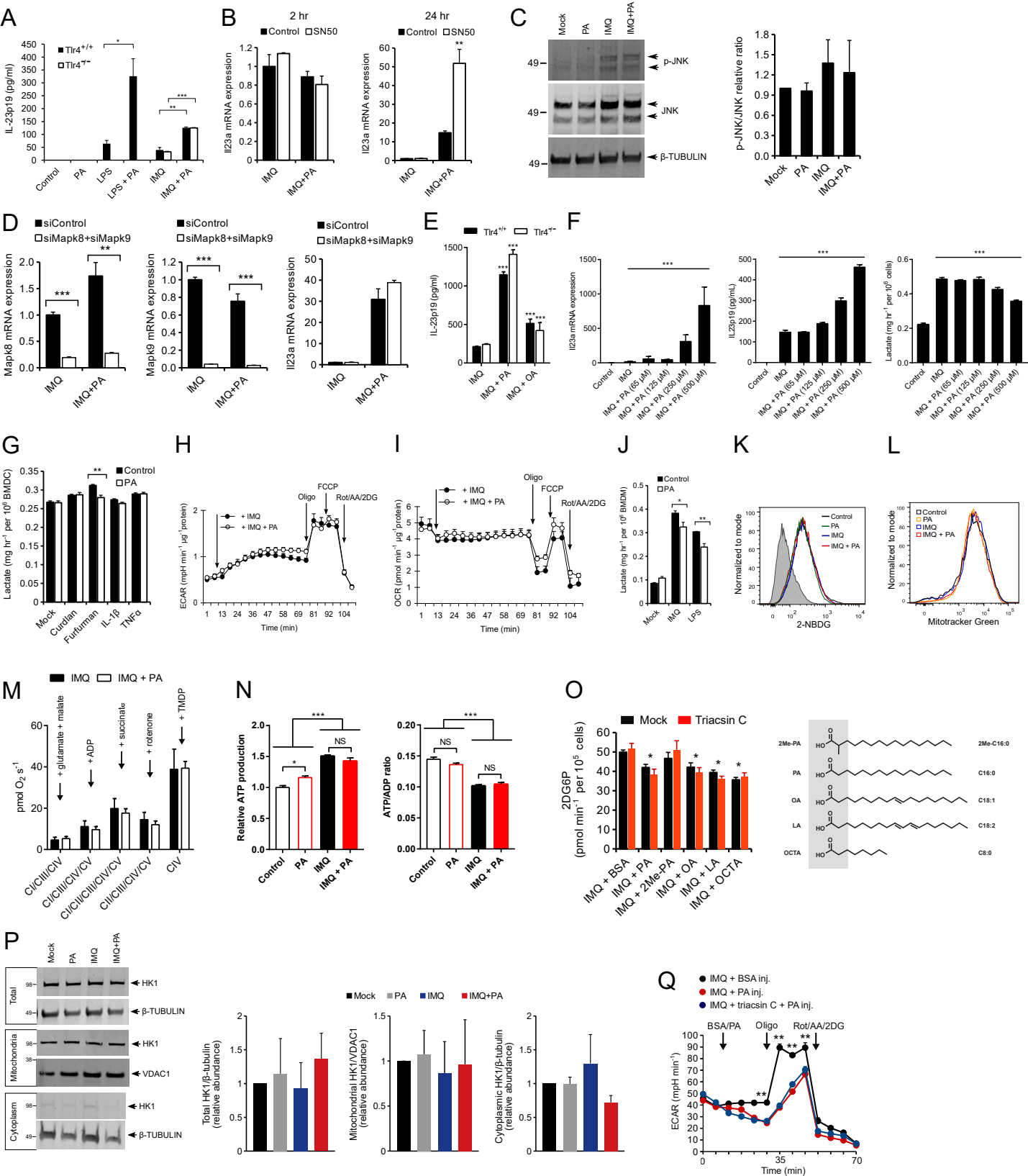
A
IL-23p19 (pg/ml)
Tlr4+/+
Tlr4−/−
Control
PA
LPS
LPS + PA
IMQ
IMQ + PA
B
2 hr
24 hr
Control
SN50
Il23a mRNA expression
IMQ
IMQ+PA
C
Mock
PA
IMQ
IMQ+PA
p-JNK
JNK
β-TUBULIN
p-JNK/JNK relative ratio
D
siControl
siMapk8+siMapk9
Mapk8 mRNA expression
Mapk9 mRNA expression
Il23a mRNA expression
E
IL-23p19 (pg/ml)
IMQ + PA
IMQ + OA
F
Il23a mRNA expression
IL23p19 (pg/mL)
Lactate (mg hr−1 per 10^6 cells)
IMQ + PA (65 μM)
IMQ + PA (125 μM)
IMQ + PA (250 μM)
IMQ + PA (500 μM)
G
Control
PA
Lactate (mg hr−1 per 10^6 BMDC)
Mock
Curdlan
Furfurman
IL-1β
TNFα
H
ECAR (mpH min−1 μg−1 protein)
+ IMQ
+ IMQ + PA
Oligo
FCCP
Rot/AA/2DG
Time (min)
I
OCR (pmol min−1 μg−1 protein)
J
Lactate (mg hr−1 per 10^6 BMDM)
K
Normalized to mode
2-NBDG
L
Mitotracker Green
M
IMQ
IMQ + PA
pmol O2 s−1
+ glutamate + malate
+ ADP
+ succinate
+ rotenone
+ TMDP
CI/CIII/CIV
CI/CIII/CIV/CV
CI/CII/CIII/CIV/CV
CII/CIII/CIV/CV
CIV
N
Relative ATP production
ATP/ADP ratio
NS
O
Mock
Triacsin C
2DG6P (pmol min−1 per 10^5 cells)
IMQ + BSA
IMQ + PA
IMQ + 2Me-PA
IMQ + OA
IMQ + LA
IMQ + OCTA
2Me-PA
PA
OA
LA
OCTA
2Me-C16:0
C16:0
C18:1
C18:2
C8:0
P
Total
Mitochondria
Cytoplasm
HK1
β-TUBULIN
VDAC1
Total HK1/β-tubulin (relative abundance)
Mitochondrial HK1/VDAC1 (relative abundance)
Cytoplasmic HK1/β-tubulin (relative abundance)
Q
IMQ + BSA inj.
IMQ + PA inj.
IMQ + triacsin C + PA inj.
BSA/PA
Oligo
Rot/AA/2DG
ECAR (mpH min−1)
Time (min)

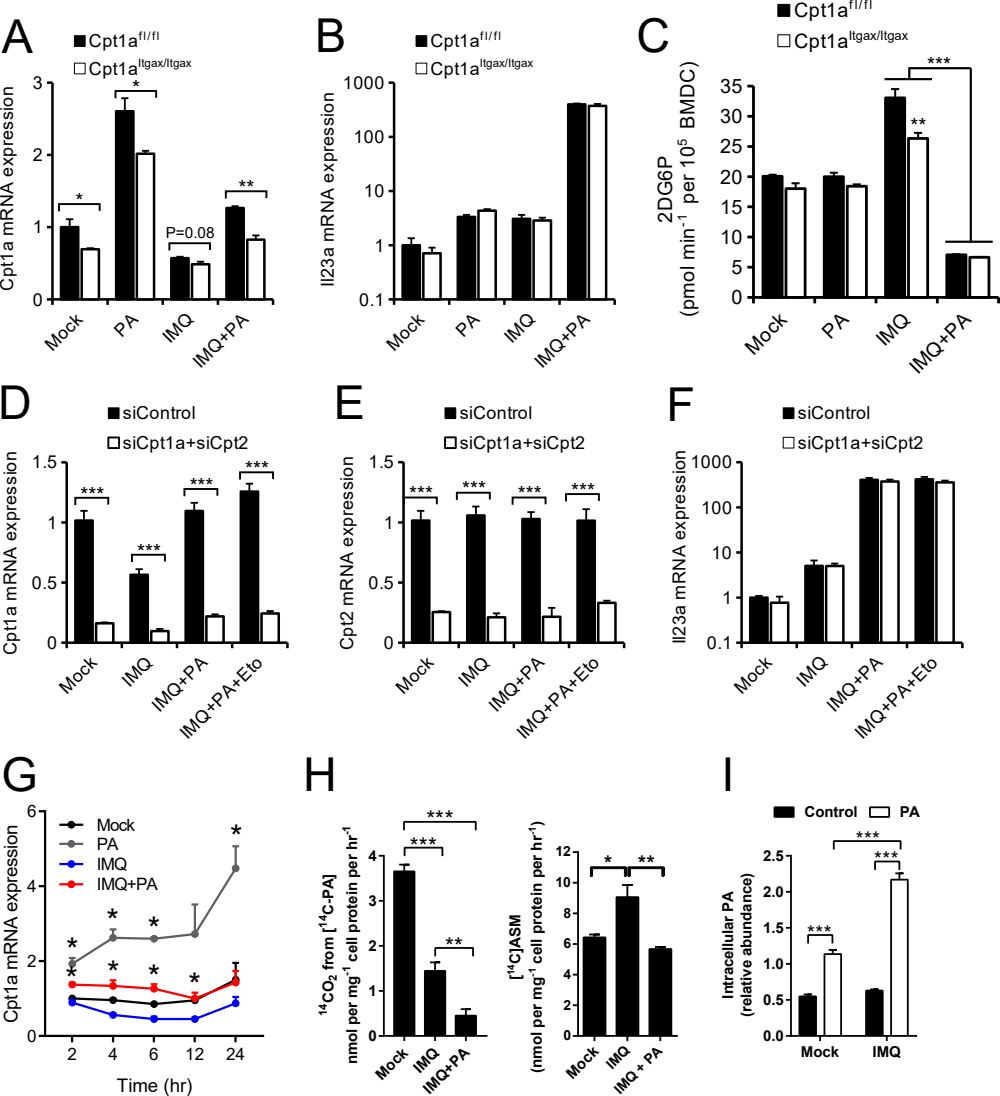
A
Cpt1a^fl/fl
Cpt1a^Itgax/Itgax
Cpt1a mRNA expression
P=0.08
Mock
PA
IMQ
IMQ+PA
B
Cpt1a^fl/fl
Cpt1a^Itgax/Itgax
Il23a mRNA expression
C
Cpt1a^fl/fl
Cpt1a^Itgax/Itgax
2DG6P (pmol min^-1 per 10^5 BMDC)
D
siControl
siCpt1a+siCpt2
Cpt1a mRNA expression
Mock
IMQ
IMQ+PA
IMQ+PA+Eto
E
siControl
siCpt1a+siCpt2
Cpt2 mRNA expression
F
siControl
siCpt1a+siCpt2
Il23a mRNA expression
G
Mock
PA
IMQ
IMQ+PA
Cpt1a mRNA expression
Time (hr)
H
14CO2 from [14C-PA] nmol per mg-1 cell protein per hr-1
[14C]ASM (nmol per mg-1 cell protein per hr-1)
I
Control
PA
Intracellular PA (relative abundance)
Mock
IMQ

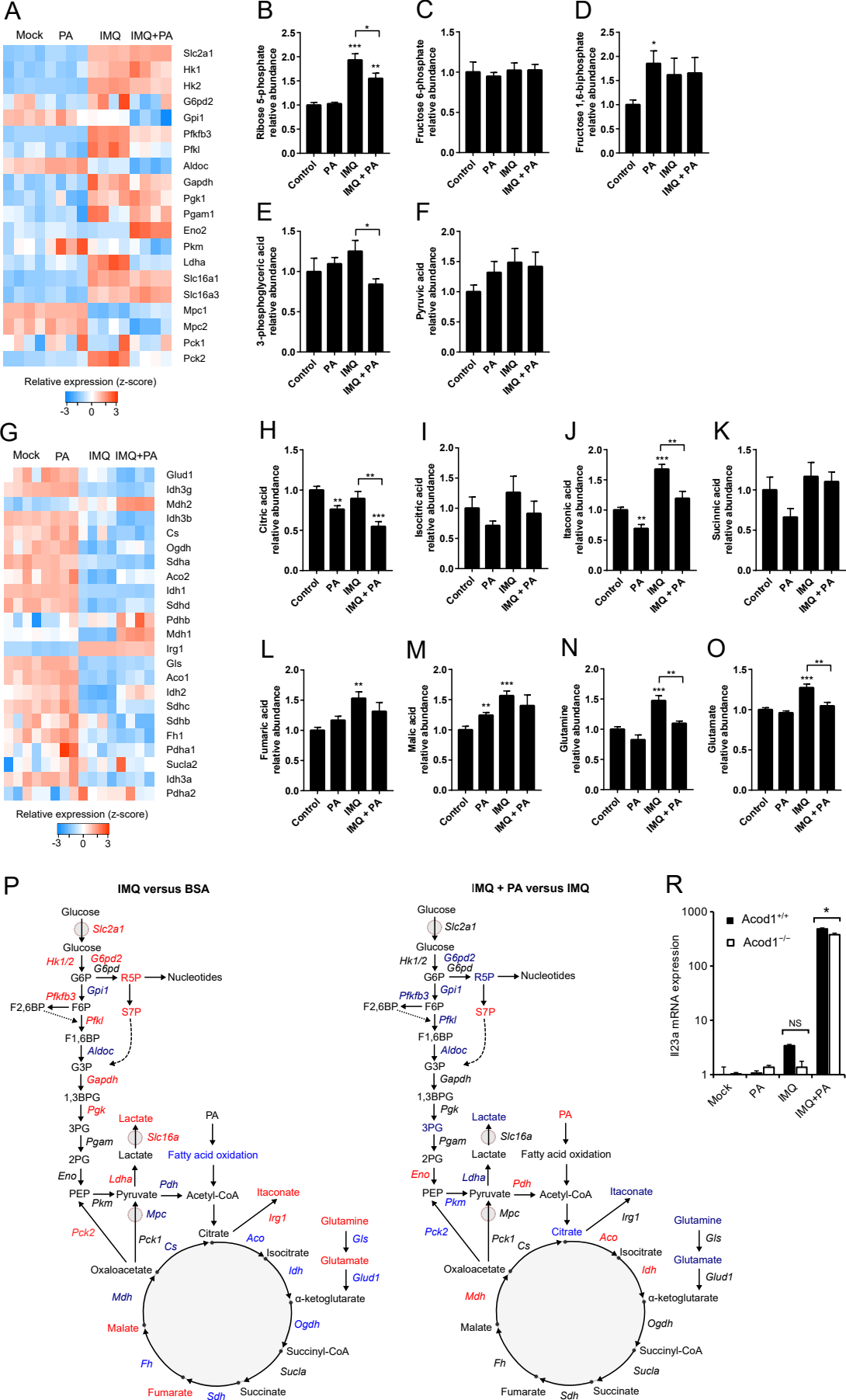
A
Mock
PA
IMQ
IMQ+PA
Slc2a1
Hk1
Hk2
G6pd2
Gpi1
Pfkfb3
Pfkl
Aldoc
Gapdh
Pgk1
Pgam1
Eno2
Pkm
Ldha
Slc16a1
Slc16a3
Mpc1
Mpc2
Pck1
Pck2
Relative expression (z-score)
-3
0
3
B
Ribose 5-phosphate relative abundance
C
Fructose 6-phosphate relative abundance
D
Fructose 1,6-biphosphate relative abundance
E
3-phosphoglyceric acid relative abundance
F
Pyruvic acid relative abundance
Control
PA
IMQ
IMQ + PA
G
Mock
PA
IMQ
IMQ+PA
Glud1
Idh3g
Mdh2
Idh3b
Cs
Ogdh
Sdha
Aco2
Idh1
Sdhd
Pdhb
Mdh1
Irg1
Gls
Aco1
Idh2
Sdhc
Sdhb
Fh1
Pdha1
Sucla2
Idh3a
Pdha2
Relative expression (z-score)
-3
0
3
H
Citric acid relative abundance
I
Isocitric acid relative abundance
J
Itaconic acid relative abundance
K
Sucinnic acid relative abundance
L
Fumaric acid relative abundance
M
Malic acid relative abundance
N
Glutamine relative abundance
O
Glutamate relative abundance
P
IMQ versus BSA
Glucose
Slc2a1
Glucose
Hk1/2
G6pd2
G6pd
G6P
R5P
Nucleotides
Gpi1
Pfkfb3
F2,6BP
F6P
Pfkl
S7P
F1,6BP
Aldoc
G3P
Gapdh
1,3BPDG
Pgk
3PG
Lactate
Slc16a
PA
Pgam
Lactate
Fatty acid oxidation
2PG
Eno
Ldha
Pdh
PEP
Pyruvate
Acetyl-CoA
Itaconate
Pkm
Mpc
Irg1
Pck2
Pck1
Citrate
Aco
Glutamine
Gls
Cs
Isocitrate
Glutamate
Oxaloacetate
Idh
Glud1
Mdh
α-ketoglutarate
Malate
Ogdh
Succinyl-CoA
Fh
Sucla
Fumarate
Sdh
Succinate
IMQ + PA versus IMQ
R
Il23a mRNA expression
Acod1+/+
Acod1−/−
NS
Mock
PA
IMQ
IMQ+PA

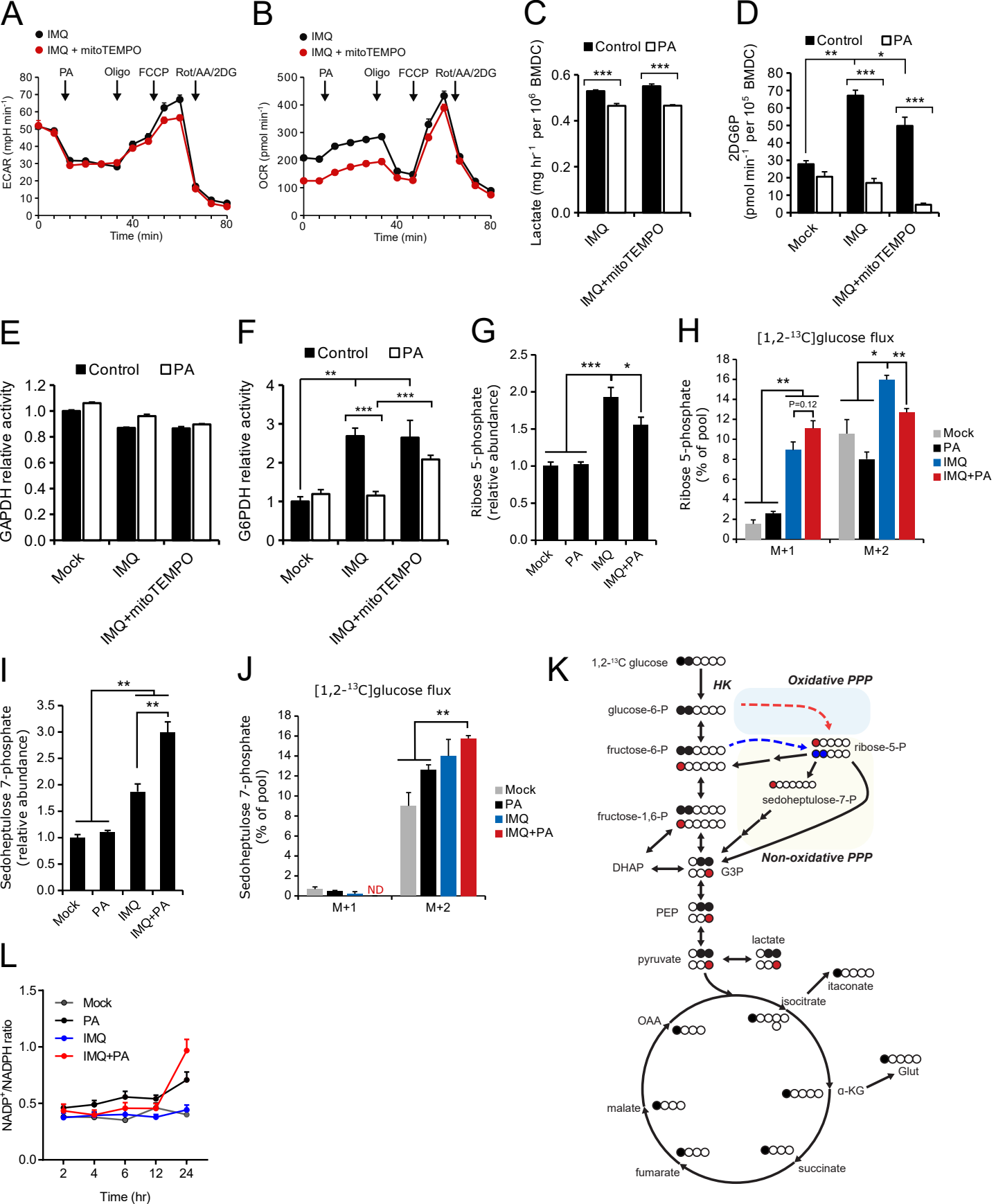
A
IMQ
IMQ + mitoTEMPO
PA
Oligo
FCCP
Rot/AA/2DG
ECAR (mpH min-1)
Time (min)
B
OCR (pmol min-1)
C
Control
PA
Lactate (mg hr-1 per 10^6 BMDC)
IMQ
IMQ+mitoTEMPO
D
2DG6P (pmol min-1 per 10^5 BMDC)
Mock
E
GAPDH relative activity
F
G6PDH relative activity
G
Ribose 5-phosphate (relative abundance)
PA
H
[1,2-13C]glucose flux
Ribose 5-phosphate (% of pool)
P=0.12
M+1
M+2
I
Sedoheptulose 7-phosphate (relative abundance)
J
Sedoheptulose 7-phosphate (% of pool)
ND
K
1,2-13C glucose
HK
Oxidative PPP
glucose-6-P
fructose-6-P
ribose-5-P
sedoheptulose-7-P
fructose-1,6-P
DHAP
G3P
Non-oxidative PPP
PEP
pyruvate
lactate
itaconate
isocitrate
OAA
α-KG
Glut
malate
fumarate
succinate
L
NADP+/NADPH ratio
Time (hr)

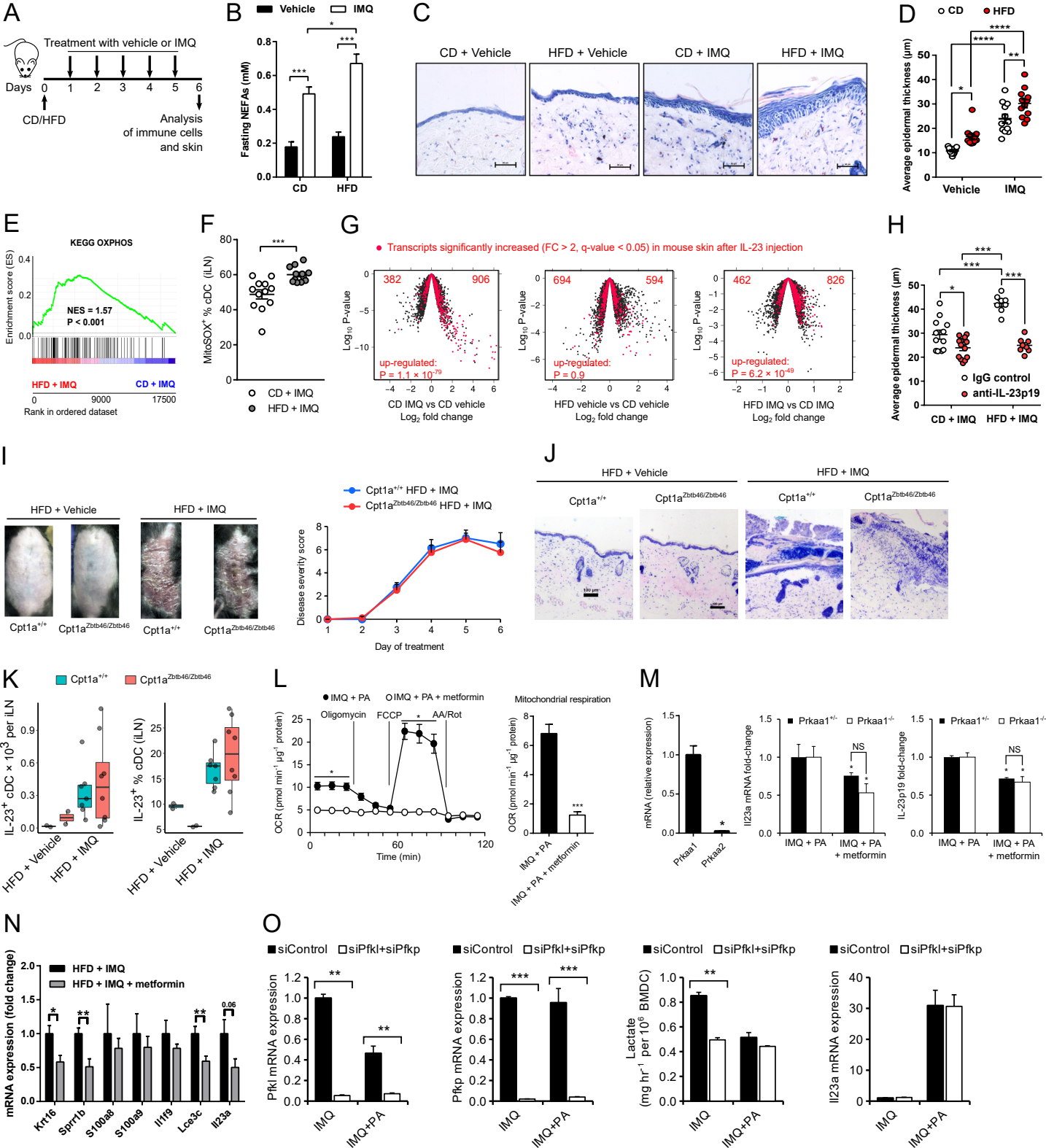
A
Treatment with vehicle or IMQ
Days 0 1 2 3 4 5 6
CD/HFD
Analysis of immune cells and skin
B
Vehicle
IMQ
Fasting NEFAs (mM)
CD
HFD
C
CD + Vehicle
HFD + Vehicle
CD + IMQ
HFD + IMQ
D
CD
HFD
Average epidermal thickness (μm)
Vehicle
IMQ
E
KEGG OXPHOS
Enrichment score (ES)
NES = 1.57
P < 0.001
HFD + IMQ
CD + IMQ
Rank in ordered dataset
F
MitoSOX+ % cDC (iLN)
CD + IMQ
HFD + IMQ
G
Transcripts significantly increased (FC > 2, q-value < 0.05) in mouse skin after IL-23 injection
382
906
up-regulated:
P = 1.1 × 10-79
694
594
up-regulated:
P = 0.9
462
826
up-regulated:
P = 6.2 × 10-49
Log10 P-value
CD IMQ vs CD vehicle Log2 fold change
HFD vehicle vs CD vehicle Log2 fold change
HFD IMQ vs CD IMQ Log2 fold change
H
Average epidermal thickness (μm)
IgG control
anti-IL-23p19
CD + IMQ
HFD + IMQ
I
HFD + Vehicle
HFD + IMQ
Cpt1a+/+
Cpt1aZbtb46/Zbtb46
Cpt1a+/+ HFD + IMQ
Cpt1aZbtb46/Zbtb46 HFD + IMQ
Disease severity score
Day of treatment
J
HFD + Vehicle
HFD + IMQ
Cpt1a+/+
Cpt1aZbtb46/Zbtb46
K
Cpt1a+/+
Cpt1aZbtb46/Zbtb46
IL-23+ cDC × 10³ per iLN
IL-23+ % cDC (iLN)
HFD + Vehicle
HFD + IMQ
L
IMQ + PA
IMQ + PA + metformin
Oligomycin
FCCP
AA/Rot
OCR (pmol min-1 μg-1 protein)
Time (min)
Mitochondrial respiration
M
mRNA (relative expression)
Prkaa1
Prkaa2
Prkaa1+/-
Prkaa1-/-
Il23a mRNA fold-change
IL-23p19 fold-change
NS
IMQ + PA
IMQ + PA + metformin
N
HFD + IMQ
HFD + IMQ + metformin
mRNA expression (fold change)
Krt16
Sprr1b
S100a8
S100a9
Il1f9
Lce3c
Il23a
O
siControl
siPfkl+siPfkp
Pfkl mRNA expression
Pfkp mRNA expression
Lactate (mg hr-1 per 10⁶ BMDC)
Il23a mRNA expression
IMQ
IMQ+PA

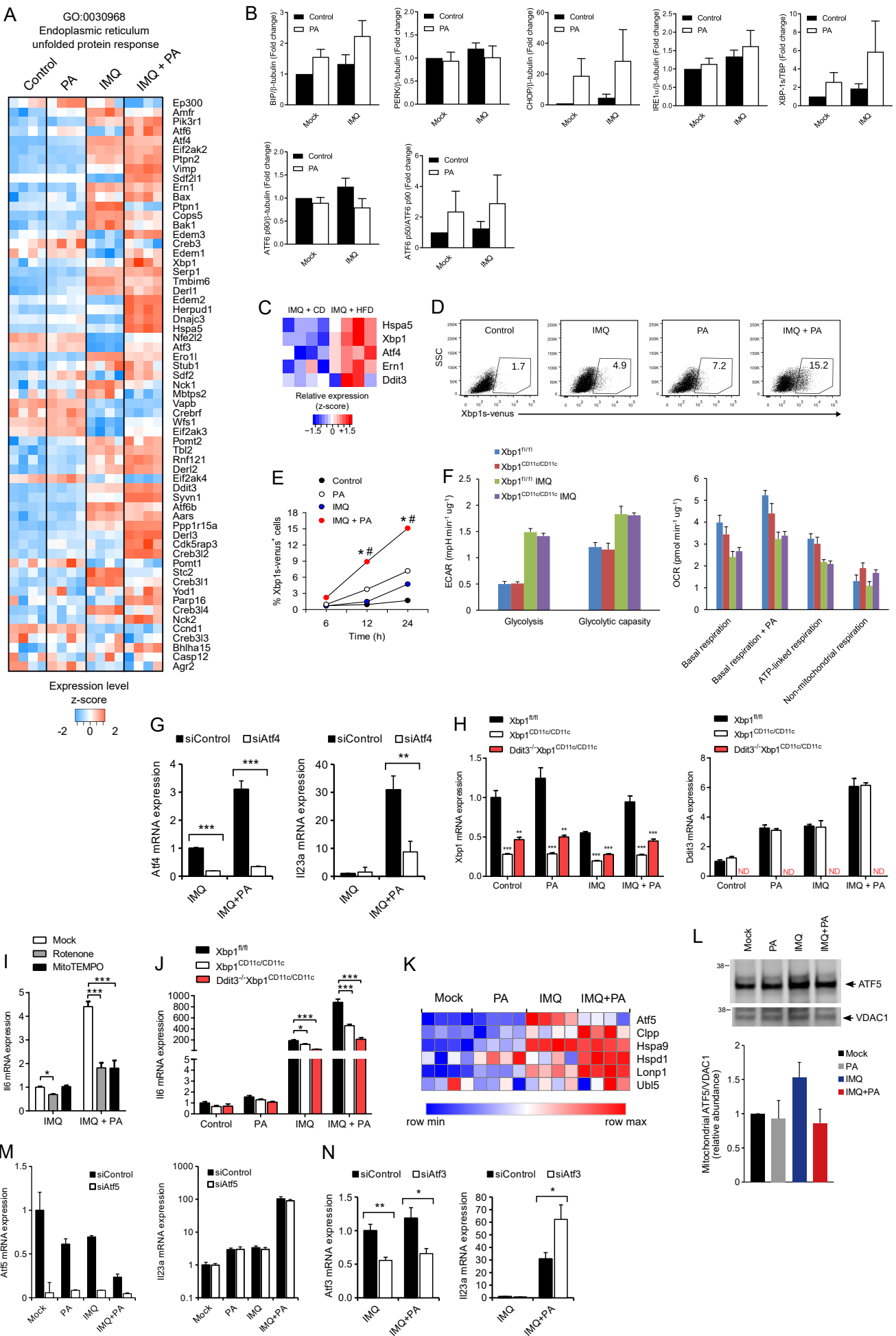
A
GO:0030968
Endoplasmic reticulum
unfolded protein response
Control
PA
IMQ
IMQ + PA
Ep300
Amfr
Pik3r1
Atf6
Atf4
Eif2ak2
Ptpn2
Vimp
Sdf2l1
Ern1
Bax
Ptpn1
Cops5
Bak1
Edem3
Creb3
Edem1
Xbp1
Serp1
Tmbim6
Derl1
Edem2
Herpud1
Dnajc3
Hspa5
Nfe2l2
Atf3
Ero1l
Stub1
Sdf2
Nck1
Mbtps2
Vapb
Crebrf
Wfs1
Eif2ak3
Pomt2
Tbl2
Rnf121
Derl2
Eif2ak4
Ddit3
Syvn1
Atf6b
Aars
Ppp1r15a
Derl3
Cdk5rap3
Creb3l2
Pomt1
Stc2
Creb3l1
Yod1
Parp16
Creb3l4
Nck2
Ccnd1
Creb3l3
Bhlha15
Casp12
Agr2
Expression level
z-score
-2
0
2
B
BIP/β-tubulin (Fold change)
PERK/β-tubulin (Fold change)
CHOP/β-tubulin (Fold change)
IRE1α/β-tubulin (Fold change)
XBP-1s/TBP (Fold change)
ATF6 p90/β-tubulin (Fold change)
ATF6 p50/ATF6 p90 (Fold change)
Control
PA
Mock
IMQ
C
IMQ + CD
IMQ + HFD
Hspa5
Xbp1
Atf4
Ern1
Ddit3
Relative expression
(z-score)
−1.5
0
+1.5
D
Control
IMQ
PA
IMQ + PA
SSC
1.7
4.9
7.2
15.2
Xbp1s-venus
E
Control
PA
IMQ
IMQ + PA
% Xbp1s-venus+ cells
Time (h)
F
Xbp1fl/fl
Xbp1CD11c/CD11c
Xbp1fl/fl IMQ
Xbp1CD11c/CD11c IMQ
ECAR (mpH min-1 ug-1)
Glycolysis
Glycolytic capasity
OCR (pmol min-1 ug-1)
Basal respiration
Basal respiration + PA
ATP-linked respiration
Non-mitochondrial respiration
G
siControl
siAtf4
Atf4 mRNA expression
Il23a mRNA expression
IMQ
IMQ+PA
H
Xbp1fl/fl
Xbp1CD11c/CD11c
Ddit3-/-Xbp1CD11c/CD11c
Xbp1 mRNA expression
Ddit3 mRNA expression
ND
Control
PA
IMQ
IMQ + PA
I
Mock
Rotenone
MitoTEMPO
Il6 mRNA expression
IMQ
IMQ + PA
J
Xbp1fl/fl
Xbp1CD11c/CD11c
Ddit3-/-Xbp1CD11c/CD11c
Il6 mRNA expression
Control
PA
IMQ
IMQ + PA
K
Mock
PA
IMQ
IMQ+PA
Atf5
Clpp
Hspa9
Hspd1
Lonp1
Ubl5
row min
row max
L
Mock
PA
IMQ
IMQ+PA
ATF5
VDAC1
Mitochondrial ATF5/VDAC1
(relative abundance)
M
siControl
siAtf5
Atf5 mRNA expression
Il23a mRNA expression
Mock
PA
IMQ
IMQ+PA
N
siControl
siAtf3
Atf3 mRNA expression
Il23a mRNA expression
IMQ
IMQ+PA

**Supplemental Table S1**

| Gene | Forward | Reverse |
|---|---|---|
| Hprt1 | GTGATTAGCGATGATGAACC | GCAAGTCTTTCAGTCCTGTC |
| Il23a | CCAGCAGCTCTCTCGGAATC | AAGCAGAACTGGCTGTTGTC |
| Rpl4 | CTGAACCCTTACGCCAAGAC | CCTTCTCGGATTTGGTTGCC |
| Pfkfb3 | CCGCTCTCATCTGTCTCGTG | CCCACAGGATCTGGGCAAC |
| Hspa5 | TGCAGCAGGACATCAAGTTC | TACGCCTCAGCAGTCTCCTT |
| Ddit3 | CCTAGCTTGGCTGACAGAGG | CTGCTCCTTCTCCTTCATGC |
| Xbp1 | CCTGAGCCCGGAGGAGAA | CTCGAGCAGTCTGCGCTG |
| Xbp1s | GAGTCCGCAGCAGGTG | GTGTCAGAGTCCATGGGA |
| Il6 | CCACGGCCTTCCCTACTTCA | CCACGATTTCCCAGAGAACATG |
| Il12a | CAAACCAGCACATTGAAGA | AGCTCCCTCTTGTTGTGGAA |
| Hif1a | CGCCTCTGGACTTGTCTCTT | TCGACGTTCAGAACTCATCCT |
| Prkaa1 | ACCTGAGAACGTCCTGCTTGATGC | CACCTCGGGGCCTGCGTACA |
| Prkaa2 | TGCTGGATGCCCAGATGAACGC | CCTCAGGTGCTGCATAATTTGGCG |
| Gls | TGCGAACATCTGATCCCAGG | TGAATTTGGCCAGCTGAGGA |
| Gls2 | CTCGACTTGGTGACCTGCTT | GCACAATGTTGCTGCTCACA |
| Mapk8 | GTCATTCTCGGCATGGGCTA | CTGGGAACAAAACACCACCTT |
| Mapk9 | CTGGGCATGGGCTACAAAGA | TGAACTCTGCGGATGGTGTT |
| Cpt1a | ACGTTGGACGAATCGGAACA | CCATGCAGCAGAGATTTGGC |
| Cpt2 | CAACTCGTATACCCAAACCCAGTC | GTTCCCATCTTGATCGAGGACATC |
| Pfkl | CCGCTGTAAGGCCTTCACTACGAG | TTATCGATGGAGCCCACCAGACC |
| Pfkp | CCCATGGTTATGGTTCCTGCT | GTCCCACTGGCTGACTGTTT |
| Atf4 | GTGGCCAAGCACTTGAAACC | GGAAAAGGCATCCTCCTTGC |
| Atf5 | GGGCACGGCTAGAAGGAAAT | AGGCAGCGTGGAAGATTGTT |
| Atf3 | CTTCCCCAGTGGAGCCAATC | TCATTTTGCTCCAGTCTTCGC |
| Krt16 | CGGCCCACTGAGATCAAAGA | AGCTCATTCTCGTACTTGGTCC |
| Sprr1b | CCAGCGACCACACTACCTGT | TTGTTGCTCATGCAACTGTGG |
| S100a8 | CCGTCTTCAAGACATCGTTTGA | GTAGAGGGCATGGTGATTTCCT |
| S100a9 | AATGGTGGAAGCACAGTTGG | CTGGTTTGTGTCCAGGTCCTC |
| Il1f9 | TACAGCTTGGGGAAGGGAACA | TAGAGCAGACAGCGATGAACC |
| Lce3c | TCAGCACAGCCTTCTTCTCC | GCACTTTGGGGAGCACTTTG |

**Supplemental Table S2**

| Region | Forward | Reverse |
|---|---|---|
| Il23a-ChIP-SiteA | GCTTCCAACCCTCCAGATCC | ACCTTCCCAGTCCTCCAAGT |
| Il23a-ChIP-SiteB | CCTCTAGCCACAACAACCTC | CCTTCACACTAGCAGGTGACT |
| Il23a-ChIP-SiteC | TTGCATCCACGGGTAAAACC | GCTTCCCTGGGTGTTACATCA |

**KEY RESOURCES TABLE**

| REAGENT or RESOURCE | SOURCE | IDENTIFIER |
|---|---|---|
| Antibodies | | |
| GRP78 (BiP), rabbit polyclonal Ab | Abcam | Cat# ab21685 |
| PERK, clone C33E10, rabbit monoclonal Ab | Cell Signaling | Cat# 3192 |
| IRE1α, clone 14C10, rabbit monoclonal Ab | Cell Signaling | Cat# 3294 |
| GADD 153 (CHOP), rabbit polyclonal Ab | Santa Cruz | Cat# sc-575 |
| GADD 153 (CHOP), clone B-3, mouse monoclonal Ab | Santa Cruz | Cat# sc-7351 |
| TBP, clone mAbcam 51841, mouse monoclonal Ab | Abcam | Cat# ab51841 |
| β-Tubulin, clone TUB 2.1, mouse monoclonal Ab | Sigma | Cat# T5201 |
| XBP-1, rabbit polyclonal Ab | Santa Cruz | Cat# sc-7160 |
| ATF6, clone 70B1413, mouse monoclonal Ab | Abcam | Cat# ab11909 |
| Hexokinase I, clone C35C4, mouse monoclonal Ab | Cell Signaling | Cat# 2024 |
| ATF5, clone EPR18286, rabbit monoclonal Ab | Abcam | Cat# ab184923 |
| VDAC1, clone B-6, mouse monoclonal Ab | Santa Cruz | Cat# sc-390996 |
| JNK, rabbit polyclonal Ab | Cell Signaling | Cat# 9252 |
| Phospho-JNK, clone G9, mouse monoclonal Ab | Cell Signaling | Cat# 9255 |
| Normal rabbit IgG | Cell Signaling | Cat# 2729 |
| CD19 PE-CF594, clone 1D3, mouse monoclonal Ab | BD Biosciences | Cat# 562291 |
| CD3 FITC, clone 145-2C11, hamster monoclonal Ab | BD Biosciences | Cat# 562286 |
| CD64 BV711, clone X54-5/7.1, mouse monoclonal Ab | Biolegend | Cat# 139311 |
| Ly6G PE-Cy7, clone 1A8, rat monoclonal Ab | Biolegend | Cat# 127618 |
| MHCII IA/IE Alexa Fluor 700 | Biolegend | Cat# 107622 |
| CD11c APC-Cy7, clone M5/114.15.2, rat monoclonal Ab | Biolegend | Cat# 117324 |
| IL-6 PE, clone MP5-20F3, rat monoclonal Ab | Biolegend | Cat# 504504 |
| IL23p19 eFlour660, clone fc23cpg, rat monoclonal Ab | eBioscience | Cat# 50-7023-80 |
| | | |
| | | |
| | | |
| | | |
| Chemicals, Peptides, and Recombinant Proteins | | |
| Recombinant mouse GM-CSF | PeproTech | Cat# 315-03 |
| 2-NBDG | Thermo Fisher | Cat# N13195 |
| MitoTracker Green FM | Thermo Fisher | Cat# M7514 |
| MitoSOX Red | Thermo Fisher | Cat# M36008 |
| LPS from E. coli | Sigma | Cat# L3024 |
| Pam3CSK4 | InvivoGen | Cat# tlrl-pms |
| Poly(I:C) | InvivoGen | Cat# tlrl-pic |
| Imiquimod | Calbiochem | Cat CAS 99001-02-6 |
| Curdlan | InvivoGen | Cat# tlrl-curd |
| Furfurman | InvivoGen | Cat# tlrl-ffm |
| SN50 | Enzo | Cat# BML-P600-0005 |
| Sodium dichloroacetate (DCA) | Tocris | Cat# 2755 |
| Triacsin C | Cayman chemical | Cat# 76896-80-5 |
| Recombinant murine TNF-α | PeproTech | Cat# 315-01A |

| | | |
|---|---|---|
| Recombinant murine IL-1β | PeproTech | Cat# 211-11B |
| MitoPQ | Abcam | Cat# ab146819 |
| Palmitic acid | Sigma | Cat# P0500 |
| Oleic acid | Sigma | Cat# O1008 |
| 2-methylhexadecanoic acid | Sigma | Cat# PH010298 |
| Linoleic acid | Sigma | Cat# L1376 |
| Octanoic acid | Sigma | O3907 |
| Bovine serum Albumin, essentially fatty acid free | Sigma | Cat# A6003 |
| Etomoxir | Sigma | Cat# E1905 |
| 2-deoxy-D-glucose | Sigma | Cat# D6134 |
| Rotenone | Sigma | Cat# R8875 |
| Metformin | Sigma | Cat# D150959 |
| MitoTEMPO | Sigma | Cat# SML0737 |
| 4μ8C | Tocris | Cat# 4479 |
| GSK2606414 | Calbiochem | Cat# CAS 1337531-89-1 |
| Tunicamycin | Sigma | Cat# SMB00071 |
| Glucose | Sigma | Cat# G8769 |
| RIPA buffer | Cell Signaling | Cat# 9806 |
| Complete Protease inhibitor cocktail | Sigma | Cat# 00000001169749800 1 |
| PhosSTOP | Sigma | Cat# 00000004906845001 |
| Control “Lanette” cream | Fagron | Cat# 1289-511 |
| HyClone Fetal calf serum (FCS) | GE Healthcare | Cat# SH30071 |
| Critical Commercial Assays | | |
| Zombie UV Fixable Viability Kit | Biolegend | Cat# 423107 |
| Ovation Pico WTA System V2 | NuGen | Cat# 3302 |
| GeneChip WT PLUS Reagent Kit | Affymetrix | Cat# 902118 |
| GeneChip WT Terminal Labeling Kit | Affymetrix | Cat# 900720 |
| GeneChip Mouse Gene 2.0 ST Array | Affymetrix | Cat# 902500 |
| Pierce Protein A/G magnetic beads | Thermo Fisher | Cat# 88802 |
| Agencourt AMPure | Beckman Coulter | Cat# A63880 |
| Mouse IL-23 DuoSet ELISA | R&D Systems | Cat# DY1887 |
| RNAaeasy Micro Kit | Qiagen | Cat# 74004 |
| Dnase I, Rnase-free | Thermo Fisher | Cat# EN0521 |
| High-capacity cDNA reverse transcription kit | Thermo Fisher | Cat# 4319983 |
| NuPAGE LDS Sample buffer | Thermo Fisher | Cat# NP0007 |
| NuPAGE 4-12% Bis-Tris Protein Gel | Thermo Fisher | Cat# NP0321BOX |
| iBlot 2 nitrocellulose Transfer stacks | Thermo Fisher | Cat# IB23001 |
| Lactate Assay Kit | Trinity Biotech | Cat# 735-10 |
| GSH-Glo™ Glutathione Assay | Promega | Cat# V6911 |
| Glucose Uptake-Glo™ Assay | Promega | Cat# J1341 |
| Glucose-6-Phosphate Dehydrogenase Activity Assay | Cayman | Cat# 700300 |
| KDalert™ GAPDH Assay | Thermo Fischer | Cat# AM1639 |
| ADP/ATP Ratio Assay Kit | Abcam | Cat# ab65313 |
| Trizol reagent | Thermo Fisher | Cat# A33251 |

| | | |
|---|---|---|
| Mouse Dendritic Cell Nucleofector Kit / Nucleofector II/2b | Lonza | Cat# VPA-1011 |
| Seahorse XF Cell Mito Stress Test Kit | Agilent Technologies | Cat# 103015-100 |
| SYBR Green Master Mix | Diagenode | Cat# DMMLD2D600 |
| Deposited Data | | |
| Mouse skin microarray data | This paper | GSE68750 |
| GM-DC microarray data | This paper | GSE110962 |
| cDC microarray data | This paper | GSE110963 |
| Experimental Models: Cell Lines | | |
| Bone marrow-derived dendritic cells differentiated in the presence of GM-CSF (GM-DC) | This paper | N/A |
| Experimental Models: Organisms/Strains | | |
| Mouse: $Tlr4^{-/-}$: B6.B10ScN-Tlr4lps-del/JthJ | Institut Pasteur de Lille, France | 007227 |
| Mouse: $Acod1^{-/-}$ : C57BL/6NJ-Acod1em1(IMPC)J/J | Institut Pasteur de Lille, France | MGI:5749792 |
| Mouse: $Prkaa1^{+/-}$: 129S2/SvPas-$Prkaa1^{tm1Sbj}$ | Institut Cochin, Rene Descartes University, Paris, France | MGI:3029359 |
| Mouse: $Prkaa1^{-/-}$: 129S2/SvPas-$Prkaa1^{tm1Sbj}$ | Institut Cochin, Rene Descartes University, Paris, France | MGI:3029359 |
| Mouse: $Hif1a^{Vav/Vav}$: B6.129-Hif1atm3Rsjo/J; (CBA/Ca x C57BL/10)F2-Tg(Vav1-icre)A2Kio | MRC Centre for Regenerative Medicine, University of Edinburgh, UK | N/A |
| Mouse: $Hif1a^{fl/fl}$Rosa26CreE: B6.129-Hif1atm3Rsjo/J; B6-129-Gt(ROSA)26Sortm1(cre/ERT)Nat/J; | Department of Molecular Medicine and Gene Therapy, Lund Stem Cell Center, Sweden | N/A |
| Mouse: $Ddit3^{-/-}$: B6.129S(Cg)-Ddit3tm2.1Dron/J | Division of Molecular Biology. Institute for Genome Research, Tokushima University, Japan | 005530 |
| Mouse: $Xbp1^{CD11c/CD11c}$: 129S6/SvEvTac-Xbp1tm2Glm; B6.Cg-Tg(Itgax-cre)1-1Reiz/J | VIB Center for Inflammation, Gent University, Belgium; or Department of Medicine, Weill Cornell Medical College, New York, USA | N/A |
| Mouse: $Ddit3^{-/-}Xbp1^{CD11c/CD11c}$: B6.129S(Cg)-Ddit3tm2.1Dron/J; 129S6/SvEvTac-Xbp1tm2Glm; B6.Cg-Tg(Itgax-cre)1-1Reiz/J | VIB Center for Inflammation, Gent University, Belgium | N/A |
| Mouse: ERAi: Tg(CAG-XBP1*/Venus)#Miur | VIB Center for Inflammation, Gent University, Belgium | MGI:4939273 |

| | | |
|---|---|---|
| Mouse: Hif1a$^{Tie2/Tie2}$: B6.129-Hif1atm3Rsjo/J; (B6.Cg-Tg(Tek-cre)1Ywa/J | William Harvery Research Institutes, Queen Mary University London, UK | N/A |
| Mouse: Cpt1a$^{Itgax/Itgax}$: Cpt1atm1.1Pec; B6.Cg-Tg(Itgax-cre)1-1Reiz/J | Institute of Infection Immunology, Hannover, Germany | N/A |
| Mouse: Cpt1a$^{Zbtb46/Zbtb46}$: Cpt1atm1.1Pec; Zbtb46tm1Kmm/J | William Harvery Research Institutes, Queen Mary University London, UK | N/A |
| Mouse: WT: C57BL/6J | Charles River | 027 |
| Oligonucleotides | | |
| Mouse Cpt1a siRNA | Dharmacon | Cat# M-042456 |
| Mouse Cpt2 siRNA | Dharmacon | Cat# M-043177 |
| Mouse Pfkl siRNA | Dharmacon | Cat# M-060388 |
| Mouse Pfkp siRNA | Dharmacon | Cat# M-059341 |
| Mouse Atf3 siRNA | Dharmacon | Cat# M-058604 |
| Mouse Atf4 siRNA | Dharmacon | Cat# M-042737 |
| Mouse Atf5 siRNA | Dharmacon | Cat# M-045123 |
| Mouse Mapk8 siRNA | Dharmacon | Cat# M-040128 |
| Mouse Mapk9 siRNA | Dharmacon | Cat# M-040134 |
| Mouse Gls siRNA | Dharmacon | Cat# M-043336 |
| Mouse Gls2 siRNA | Dharmacon | Cat# M-063540 |
| SiGENOME non-targeting siRNA pool #1 | Dharmacon | Cat# D-001206 |
| Mouse Pfkfb3 siRNA | OriGene | Cat# SR416726 |
| Universal scrambled negative control siRNA | OriGene | Cat# SR30004 |
| Mouse qPCR Primers, see Table S1 | N/A | N/A |
| ChIP-qPCR Primers, see Table S2 | N/A | N/A |
| Recombinant DNA | | |
| | | |
| Software and Algorithms | | |
| Prism version 6 | GraphPad | N/A |
| GSEA Desktop v3.0 | Broad Institute | http://software.broadinstitute.org/gsea/index.jsp |
| Affy version 1.60.0 | Bioconductor | http://bioconductor.org/packages/release/bioc/html/affy.html |
| Limma version 3.38.3 | Bioconductor | http://bioconductor.org/packages/release/bioc/html/limma.html |
| FlowJo version 8 | Tree Star | https://www.flowjo.com/ |

| | | |
|---|---|---|
| Phantasus | Artyomov Lab, Washington University in St. Louis | https://artyomovlab.wustl.edu/phantasus/ |
| Diva version 7.0 | Becton Dickinson | http://www.bdbiosciences.com/us/instruments/research/software/flow-cytometry-acquisition/bd-facsdiva-software/m/111112/overview |
| | | |
| Other | | |
| High Fat Diet (HFD; 60% kcal fat) | Research diets | Cat# D12492 |
| Aldara 5% IMQ cream | Meda AB | N/A |
| | | |
| | | |
| | | |
| | | |
| | | |
| DMEM media | Thermo Fisher | Cat# 11960044 |
| | | |
| | | |
| | | |
| Mitochondrial Respirometry Solution (*MiR05*) | Oroboros Instruments | # 60101-01 http://www.bioblast.at/index.php/MiR05-Kit |
| | | |
| ImmunoHistoFix | Gentaur | # amp-202 |
| ImmunoHistoWax | Gentaur | # amp-201 |